Contents list available at CBIORE journal website

International Journal of Renewable Energy Development

Journal homepage: https://ijred.cbiore.id

Research Article

Techno-economic feasibility analysis of hybrid renewable energy system for off-grid African communities: Insights from a Zambian case study

Satnam Singh Virdy[a], Francis D.Yamba[a], Manish Mishra[b], Isaac N. Simate[c], Mala Ramesh[d], Mwansa Kaoma[c], Edwin Luwaya[a], Simon Tembo[e], Shabbir H. Gheewala[f,g,*]

[a]*Department of Mechanical Engineering, School of Engineering, University of Zambia, Zambia*

[b]*Department of Mechanical Engineering, Indian Institute of Technology Roorkee, Uttarakhand, India*

[c]*Department of Agricultural Engineering, School of Engineering, University of Zambia, Zambia*

[d]*Department of Electrical and Electronics Engineering, Malnad College of Engineering, Hassan, Karnataka, India*

[e]*Department of Electrical and Electronics Engineering, School of Engineering, University of Zambia, Zambia*

[f]*The Joint Graduate School of Energy and Environment, King Mongkut's University of Technology Thonburi, Bangkok, Thailand*

[g]*Center of Excellence on Energy Technology and Environment, Ministry of Higher Education, Science, Research and Innovation, Bangkok, Thailand*

Abstract. As hybrid renewable energy systems are increasingly adopted for rural electrification, this study presents an approach for optimizing off-grid systems in resource-abundant regions. Using a Zambian case study, this study demonstrates actionable insights into the optimal selection and configuration of components for a renewable energy-based off-grid system designed for remote, unelectrified communities with access to solar, wind, and biomass resources. The system's technical, economic, and environmental performance was evaluated through simulation in HOMER Pro software, using various photovoltaic panel ratings (335W, 400W, and 445W), battery technologies (lead-acid, lead-carbon, and lithium-ion), and dispatch strategies (load-following, cycle-charging, predictive-dispatch, and combined-dispatch). Among several configurations, the one featuring a 445W photovoltaic panel and a lithium-ion battery operating under the load-following strategy demonstrated the lowest cost and highest environmental benefits. This configuration resulted in a total lifetime system cost of USD 3.857 million and a levelized cost of electricity of 0.1522 USD per kilowatt-hour, while reducing emissions by 99.9% compared to a diesel-only system. Sensitivity analysis, considering ±20% variations in component costs and discount rate, showed that battery cost had the largest influence, causing a 5 to 12% variation in system cost. These findings suggest that combining high-efficiency solar panels with advanced battery storage and an appropriate dispatch strategy can significantly enhance the affordability and sustainability of off-grid renewable energy systems for rural communities worldwide.

Keywords: Hybrid renewable energy system, dispatch strategies, Homer Pro, Techno-economic optimization, Zambian.

Received: 15th May 2025; Revised: 26th Oct 2025; Accepted: 6th Dec 2025; Available online: 29th Dec 2025

1. Introduction

The need for reliable access to energy plays a vital role in providing socioeconomic services to improve the social quality of life in any society. However, developing countries are faced with energy shortages in remote regions lacking grid supply. In this regard, Target 7.1 of the Sustainable Development Goal (SDG) No. 7 of the 2030 Agenda for Sustainable Development, strives to "guarantee access to reliable, affordable and modern-day energy services universally". Target 7.2 further strives to "substantially increase the portion of green energy in the world energy mix" (UN SDG Report, 2023). Saha *et al.* (2022) stateed that about 85% of the global energy is currently obtained from non-renewable sources and that in the near future, such resources will not be able to meet the desired demand due to their rapid rate of depletion. In response to the aforementioned facts, Ganjei *et al.* (2022) reported that many countries around the world are increasingly planning to employ renewable energy sources (RES) to accomplish the energy demands of remote communities. The Zambian National Energy Policy of 2019 also recognizes that energy is the largest commodity market in the world and the need to manage it sustainably is increasingly becoming important (Ministry of Energy, 2019). The 2021 World Bank Collection of Indicators reported that power supply is accessible to only about 47% of the Zambian populace with urban areas standing at 86%, while for rural areas, accessibility to power supply stood at a mere 14.5% (World Bank Open Data Energy Progress Report, 2023). The 2023 SDG Tracking Report states that although the world continues to advance towards sustainability targets, the pace is not fast enough to achieve the set targets (UN SDG Report, 2023).

It is well known that rural grid extension faces significant challenges due to rough terrain, low consumption, low

* Corresponding author
Email: shabbir.ghe@kmutt.ac.th (S.H. Gheewala)

https://doi.org/10.61435/ijred.2026.61421
ISSN: 2252-4940/© 2026.The Author(s). Published by CBIORE

household earnings, underdeveloped transportation infrastructures, distributed consumer colonies, etc. (Sudarsan and Sreenivasan, 2022). As a result, residents of rural areas resort to diesel generators to meet their electricity demand. However, this mode of generation not only requires routine periodic maintenance but also poses drawbacks of causing pollution from greenhouse gas emissions and noise (Heyne *et al.,* 2022). Micangeli *et al.* (2017) observed that electricity production using diesel generators is neither economically feasible nor eco-friendly. This energy circumstance can be reformed by harnessing renewable energy resources. However, although harnessing standalone RES can provide promising solutions, their usage on a single technology basis has the disadvantage of not being able to supply power on a continuous basis due to their intermittent nature both on a daily basis and time of the year (Bansal, 2022). One way of alleviating this drawback is through utilizing Integrated Renewable Energy Sources (IRES) comprising two or more RES, that can complement the intermittency of each other (Bahramara et al., 2016). However, Khan *et al.* (2022) observed that as the capability of the RES, load demand, and economic parameters vary according to location, the design related to Hybrid Renewable Energy System (HRES) is therefore site specific. In this regard, Hassan *et al.* (2022) also emphasize that arriving at an optimal HRES design for a specific site, aspects such as size, component cost, and carbon emissions should be given special attention. Bishoge *et al.* (2019) point out that a huge biomass potential in the form of animal wastes exists in the Sub-Saharan Africa (SSA), which can be used to produce biogas to be used for off-grid generation of electricity using HRESs. This animal-based potential unfortunately remains largely untapped (Shane and Gheewala, 2017; Shane *et al.,* 2017; Gabisa and Gheewala, 2018; Kaoma and Gheewala, 2020). Consequently, not much investigation into hybrid biogas based electric systems can be found for regions within SSA. In this vein, Kaoma and Gheewala (2021a) present initial insights on sustainability performance of biomass-based systems in Zambia and recommend more in-depth investigations on the application of such systems for both cooking and electricity generation. Kaoma and Gheewala (2021b) also identify two key opportunities for deploying bio-energy systems in rural Zambia as the abundant availability of biomass and uneconomical costs of grid extension.

Energy storage is critical to the reliability and cost-effectiveness of hybrid renewable systems. Batteries not only provide backup during intermittency (Babatunde et al., 2020; Bukar *et al.,* 2019) but also reduce reliance on diesel gensets, whose use in rural areas is constrained by fuel price volatility, high operating costs, and emissions (Dhavala *et al.,* 2021; Dibaba, 2019). While coupling renewables with diesel can yield cost savings (Kumar & Saini, 2020), the broader consensus is that storage integration is essential for sustainable off-grid systems.

Existing studies have applied diverse optimization approaches to HRES design. Some have examined PV, wind, and diesel combinations (Chauhan & Saini, 2016; Bukar *et al.,* 2019), others have compared battery technologies under varying climatic or economic conditions (Biramo, 2020; Khan *et al.,* 2022), and several have investigated dispatch strategies (Ramesh & Saini, 2020; Chaurasia *et al.,* 2022). These works highlight that technology choice, particularly battery type, and control strategies strongly shape system costs and emissions. However, most investigations consider one dimension at a time (e.g., battery type, dispatch method, or PV rating) and rarely assess their combined influence.

Moreover, while there is growing work in Asia and India (e.g., Abdulkarim et al., 2018; Bhatt *et al.,* 2022), few comparable studies exist for Sub-Saharan Africa. In Zambia, despite abundant renewable and biomass potential (Virdy & Yamba, 2013), little has been done to evaluate integrated PV/WT/BG/DG/BT systems. In particular, the role of lead-carbon batteries remains underexplored relative to lead-acid and lithium-ion technologies, and the combined effects of PV panel sizing and dispatch strategies on both economics and emissions have not been systematically studied.

To address these gaps, this paper simultaneously evaluates (i) three PV panel ratings (335, 400, and 445 W), (ii) three battery technologies (lead–acid, lead–carbon, lithium-ion), and (iii) four dispatch strategies load following, Cycle Charging (CC), Combined Dispatch (CD) and Predictive Dispatch (PD) in a Zambian village context. In addition, we incorporate biogas generation, an abundant but underutilized resource in the region, and apply a multi-criteria decision analysis (MCDA) that jointly considers cost and environmental performance. This integrated approach provides more comprehensive insights for rural electrification planning than prior single-dimension studies.

2. Study Area

Two neighboring un-electrified villages, namely Bunda-Bunda North and Lyamina in Chinyunyu area, Lusaka Province in Zambia have been considered as the study area. The location lies about 90km east of Lusaka, the capital city of Zambia. The specific location of Bunda-Bunda North is -15.265791S, 29.004468E, while that for Lyamina is -15.257303S, 29.017347E. The eastern border of Lyamina village is in form of a stream from the Chinyunyu hot spring. The choice for selecting this study area was made after considering the activities taking place in the area. Bunda-Bunda North village has a clinic, secondary school, church, and a police post and road side shops. The village has 500 households, while Lyamina has about 35 households and touches the hot spring heritage center. The total number of households in the chosen is therefore 535 with an average of 6 members per household at the time of the survey, giving an estimated population of 3210The major economic activity for both villages is crop and livestock farming. the main crops grown are maize, groundnuts, tomatoes, onions, and okra, and the main animals found in the area are cattle, goats, sheep, pigs, chickens, and guinea-fowls. The two villages are also chosen as a combined community since they have similar demographic characteristics and share a common administration.

As the study area is not electrified, the main sources for lighting are candles, battery torches, and small solar lamps. As the area has abundant vegetation, the main sources for heating and cooking happen to be charcoal and firewood. The

Fig.1. Satellite map of Chinyunyu area

Table 1
Power rating of different appliances with seasonal duration of usage under each load category

Appliance	Power Rating (W)	Seasonal operating slots						No. of Appliances in each load category				Total No. of Devices
		Summer Time Slot	Summer Duration	Cool Dry Time Slot	Cool Dry Duration	Rainy Time Slot	Rainy Duration	Domestic	Commercial	Community	Agriculture	
Bulb	60	19:00 – 21:00	2	18:00 – 21:00	3	18:00 – 21:00	3	1390	57	215	-	1662
Security Light	60	19:00 – 06:00	11	19:00 – 06:00	11	19:00 – 06:00	11	536	8	23	-	567
TV	150	19:00 – 22:00	3	19:00 – 21:00	2	19:00- 21:00	2	535	2	8	-	545
Small Fan	75	12:00 – 06:00	18	12:00 – 14:00	2	20:00 – 06:00	10	535	49		-	584
Ceiling Fan	120	18:00 – 22:00	4	-	0	18:00 – 22:00	4			31	-	31
House Fridge	120	00:00 – 24:00	24	00:00 – 24:00	24	24:00 – 00:00	24	214			-	214
Large Fridge	200	00:00 – 24:00	24	00:00 – 24:00	24	24:00 – 00:00	24		7	14	-	21
Mobile Phone	10	11:00 – 14:00	3	11:00 – 14:00	3	11:00 – 14:00	3	1498	90	65	-	1653
Radio	15	08:00 – 20:00	12	10:00 – 20:00	10	10:00 – 20:00	10	535	45	9	-	589
Laptop	80	18:00 – 20:00	2	18:00 – 20:00	2	18:00 – 20:00	2	214	2		-	216
HF Radio	800	08:00 – 09:00 16:00 – 17:00	2	08:00 – 09:00 16:00 – 17:00	2	08:00 – 09:00 16:00 – 17:00	2	-		2	-	2
Music System (Bar)	360	19:00 – 24:00	5	19:00 – 24:00	5	19:00 – 24:00	5	-	2		-	2
Electric Stove (Institutions Only)	2,200	06:00 – 08:00 12:00 – 13:00 14:00 – 15:00 18:00 – 20:00	6	06:00 – 08:00 12:00 – 13:00 14:00 – 15:00 18:00 – 20:00	6	06:00 – 08:00 12:00 – 13:00 14:00 – 15:00 18:00 – 20:00	6	-	2	7	-	9
Office Equipment	8,940	08:00 – 12:00 14:00 – 16:00	6	08:00 – 12:00 14:00 – 16:00	6	08:00 – 12:00 14:00 – 16:00	6	-	-	Lumped	-	Various
Music Equipment	980	10:00 – 12:00 19:00 – 21:00	4	10:00 – 12:00 19:00 – 21:00	4	10:00 – 12:00 19:00 – 21:00	4	-	-	Lumped	-	Various
Medical Equipment	3,470	08:00 – 12:00	4	08:00 – 12:00	4	08:00 – 12:00	4	-	-	Lumped	-	Various
Dental Facility	1,200	09:00 – 10:00	1	09:00 – 10:00	1	09:00 – 10:00	1	-	-	Lumped	-	Various
Drinking Water Pumping	750	10:00 – 11:00 15:00 – 16:00	2	10:00 – 11:00 15:00 – 16:00	2	10:00 – 11:00 15:00 – 16:00	2	-	-	5	-	5
Street Light	300	19:00 – 06:00	11	19:00 – 06:00	11	19:00 – 06:00	11	-	-	30	-	30
Irrigation Water Pumping	750	15:00 – 16:00	1	15:00 – 16:00	1	15:00 – 16:00	1	-	-	-	24	24
Milling Plant	12,500	14:00 – 16:00	2	14:00 – 16:00	2	14:00 – 16:00	2	-	1	-	-	1

geographic location of the research site with the main entities considered for power supply from the designed HRES is shown in Fig. 1.

2.1. Load Assessment

A field survey was conducted to assess the load demand for the area with regard to the number of households, clinic, school,

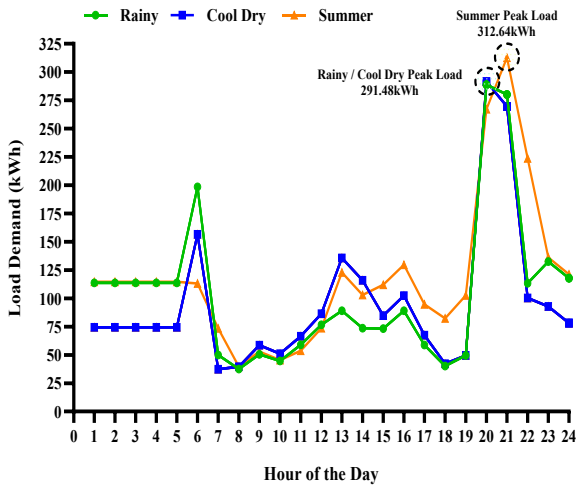

Fig.2. Daily load curves for the summer, rainy and winter seasons of the study area

church, and police post in the area. The loads were then classified as domestic, commercial, community, and agricultural loads. The domestic load comprises households. Commercial load comprises roadside shops, bars, and a milling plant. The community load comprises a church, school, health center, hot spring heritage site, and a police post. The agriculture load mainly comprises water pumps for irrigation purposes. The various electrical appliances considered for the load estimation are a bulb, a mobile phone, a radio, a TV, a laptop, a fridge, a fan, an electric stove, music equipment, office equipment, an HF radio, a street light, a water pump, and a milling plant. Detailed disaggregated tables showing appliance ownership, ratings, seasonal usage patterns, and facility-level loads for the domestic and commercial sectors are presented in Tables 1 and A1, respectively.

The daily energy consumptions for the three seasons were estimated using Eq. (1) (Ramesh and Saini, 2021):

$$E_{Demand} = \frac{\sum_{j=1}^{Type} \left(\sum_{i}^{Load} n_{Load-i,j} \times r_{rating-i,j} \times T_{Duration-i,j} \right)}{1000} \quad (1)$$

Where: E_{Demand} is the load demand (kWh), $n_{Load\text{-}i,j}$ is the number of ith load under jth type, $r_{rating\text{-}i,j}$ = rating of ith load under jth type (kW), and $T_{Duration\text{-}i,j}$ is the duration of i^{th} load under j^{th} type (hours).

The day-to-day energy consumptions are estimated as 966, 1256, and 1492 kWh/day for the rainy (Dec. – Mar.), cool-dry (Apr. – Aug.) and summer (Sep. – Nov.) seasons respectively, and the daily peak loads are estimated as 312 kW for the summer season and about 291 kW for both the rainy and cool-dry seasons. The respective load curves, showing these peak loads on a daily basis for the three seasons, are shown in Fig. 2.

2.2. Resource Assessment

This section describes how the various resources available in the study area are estimated. Fig. 3 shows the climatic data of the area.

2.2.1. Solar Resource

The resource for solar radiation was retrieved from the NASA laboratory linked within the HOMER Pro software. The annual average solar irradiation was 5.63 kWh/m^2/day. The global irradiation and clearness index of the research site are shown in Fig. 3a.

2.2.2. Wind Resource

The wind data was retrieved from the NASA laboratory linked within the HOMER software. The annual average wind speed was 5.28 m/s. The data for the wind resource of the study area is as shown in Fig. 3b.

2.2.3. Biogas Resource

The information for biogas resource has been obtained from the Ministry of Livestock and Fisheries located at a distance of 6km east of the study area. The Ministry provided the number of chickens, guinea fowls, goats, cattle, sheep, and pigs present in the area. It has been observed that collecting biomass may be a challenge because the animals and poultry in Africa tend to roam freely while grazing from place to place in search of feed. Therefore, in this study, zero grazing is assumed to estimate the collection efficiency of animal dung and poultry droppings. A gathering efficiency of 60 % is applied to determine the actual amount of animal dung and poultry droppings collected (Mwakitalima, 2023). The total daily feedstock for the area is then estimated using Eq. (2), following Werner *et al.* (1989):

$$F_{Total} = \sum_{i=1}^{n} N_i \times F_i \times \eta_g \quad (2)$$

Where: F_{Total} is the total feedstock (kg), N_i = number of animals of type i, F_i is the daily amount of feedstock produced by animal of type i (kg/day), n is the total number of different animal types, and η_g is the gathering efficiency of feedstock (taken as 0.6).

The total daily feedstock for the area was estimated as 5.25 tonnes/day.

3. Methods

Based on the resources present in the research site, i.e., solar, wind, and biomass, several HRES configurations are compared based on the economic indicators namely NPC and COE. In particular, four cases have been considered for the

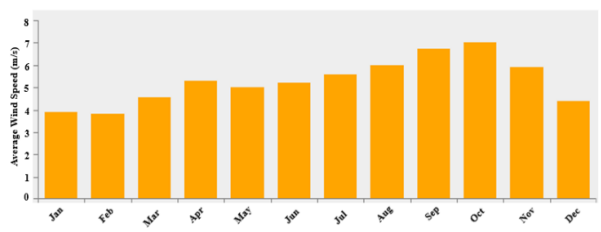

(a) Monthly solar radiation

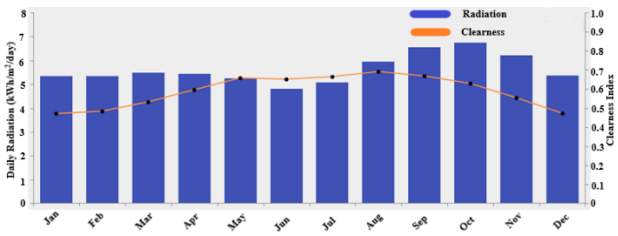

(b) Monthly wind speed

Fig. 3 Monthly climatic data for Chinyunyu area

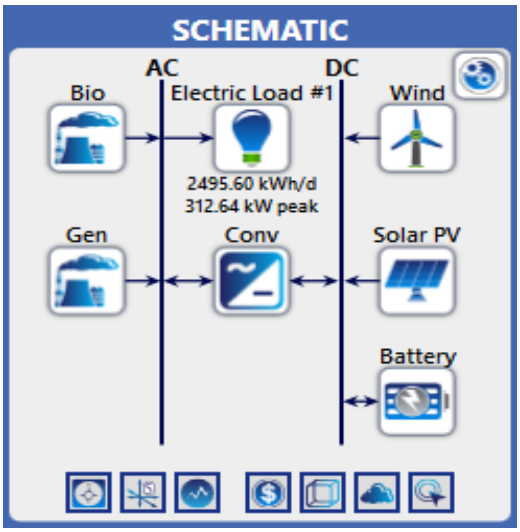

Fig. 4: Schematic representation of the proposed HRES

detailed analysis, i.e, PV/WT/DG/BG/BT, PV/DG/BT, PV/BG/BT, and PV/BT, defined as Case I, Case II, Case III, and Case IV, respectively. These are compared with the base case (DG only), In order to mitigate the effect of carbon emissions and making the system environmentally friendly, the diesel generator is omitted in the hybrid model. However, the diesel generator is used as a base case model to form a basis for the economic feasibility of the proposed HRES.

Fig.4 shows the schematic layout of the HRES configuration comprising PV array, wind turbine (WT), diesel generator (DG), biogas generator (BG), battery (BT), and bi-directional converter connected to the load. The DG is coupled to the AC-bus while the PV, WT and battery are connected to the DC-bus. The bi-directional converter is coupled to both the AC and DC buses.

The procedure adopted in the present study consists of three main phases, namely pre-HOMER data collection, HOMER simulations, and post-HOMER analysis, as shown schematically in Fig.5.The theoretical analysis required to arrive at a technically feasible solution for a real-life HRES required is quite complex. HOMER pro software is chosen in this work as it helps in simplifying the analysis to determine the optimal model within set constraints to arrive at the best solution by calculating the Net Present Costs (NPC), Cost of Electricity (COE), emissions and other relevant parameters for various solutions obtained. The load and resource estimation are performed in Phase-I. In Phase-II, HOMER is used to carry out simulations to give a number of viable designs comprising the chosen components along with the irrespective performance characteristics under specific constraints. In Phase-III, the outcomes of the various designs are compared based on their respective constraints like renewable fraction, duty factor, pollutant emissions, etc., specified in Phase-II, from which the desired solutions are selected for further analysis.

3.1. Components of the proposed HRES

This section presents the mathematical modelling of the components used in the proposed HRES.

3.1.1. Solar PV Array

The PV array uses the solar radiation to generate power. HOMER utilizes Eq. (3) to estimate the power output from the PV array as follows (Akhtari and Baneshi, 2019):

$$P_{PV} = Y_{PV} f_{PV} \left(\frac{G_T}{G_{T,STC}}\right)\left[1 + \alpha_p\left(T_C - T_{C,STC}\right)\right] \quad (3)$$

Where, Y_{PV} is the PV array's rated capacity under standard test conditions (kW), f_{PV} is the derating factor which accounts for losses due to wire losses, shadow, dirt, temperature, etc. (%), G_T is the hourly incident solar radiation at the surface of the solar PV modules under working conditions (kW/m^2), $G_{T,STC}$ is the

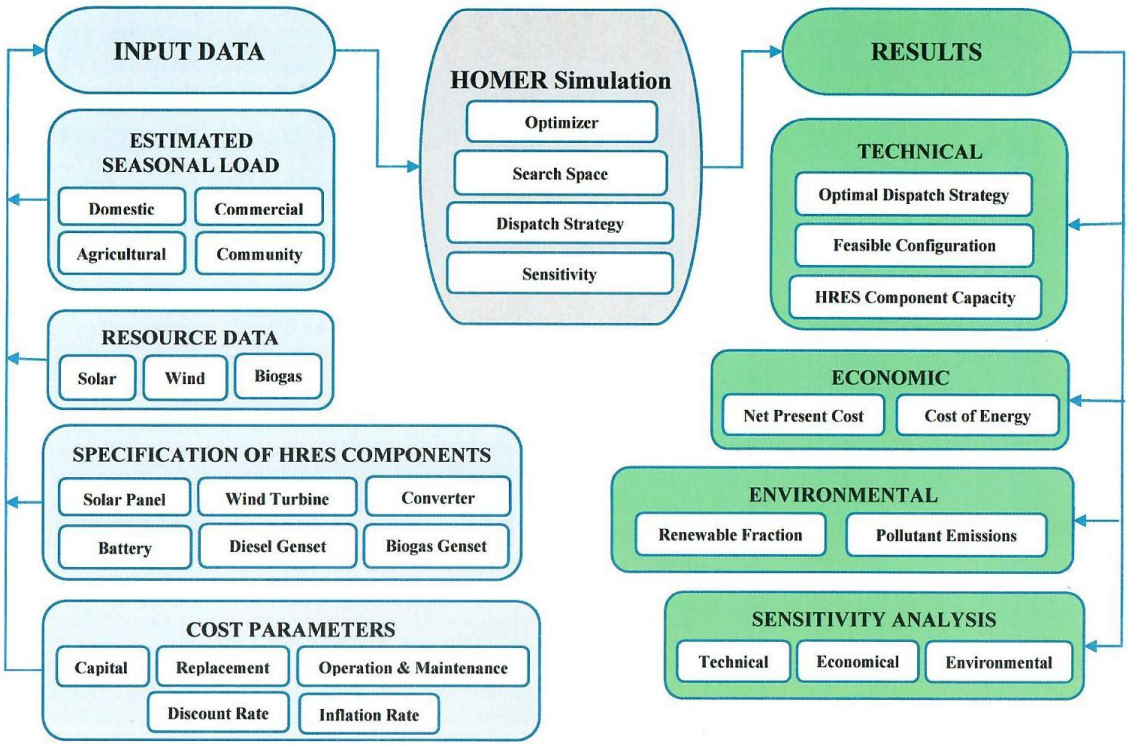

Fig. 5 Procedure adopted using HOMER software

incident radiation at standard conditions (1 kW/m^2), α_p is the temperature coefficient of power of the PV array (%/°C), T_C is the PV cell temperature under the current time step (°C), and $T_{C,STC}$ is the temperature of the PV array at standard conditions (25°C).
If the effects of temperature are insignificant, the output power from the PV array is expressed by Eq. (4) as follows (NREL, 2019):

$$\boldsymbol{P_{PV} = Y_{PV} f_{PV} \left(\frac{G_T}{G_{T,STC}}\right)} \quad (4)$$

The PV array energy balance is expressed by Eq. (5) as follows:

$$\boldsymbol{\tau\alpha G_T = \eta_c G_T + U_L (T_c - T_a)} \quad (5)$$

Where: τ is the Transmittance of the solar PV modules (%), α is the absorptance of the PV modules (%), U_L is the coefficient of heat transfer to surroundings (kW/m^2°C), and T_a is the ambient temperature (°C).

Eq. (4) can be rearranged into Eq. (6) to give the PV array cell temperature as follows:

$$\boldsymbol{T_c = T_a + G_T \left(\frac{\tau\alpha}{U_L}\right)\left(1 - \frac{\eta_c}{\tau\alpha}\right)} \quad (6)$$

Since the quantity $(\tau\alpha/U_L)$ can rarely be obtained directly by taking the values (NOCT = 0.8 kW/m^2, T_a = 20°C and η_c = 0), and expressing it in terms of the Nominal Operating Cell Temperature (NOCT) as in Eq. (7):

$$\boldsymbol{\frac{\tau\alpha}{U_L} = \frac{T_{c,NOCT} - T_{a,NOCT}}{G_{T,NOCT}}} \quad (7)$$

Where, $T_{C,NOCT}$ is the Nominal Operating Cell Temperature, $T_{a,NOCT}$ is the ambient temperature at NOCT, and $G_{T,NOCT}$ is the solar radiation at NOCT.

Taking $(\tau\alpha/U_L)$ as a constant and $(\tau\alpha = 0.9)$, Eq. (6) can be inserted into Eq. (5) to express T_C as Eq. (8):

$$\boldsymbol{T_c = T_a + G_t \left(\frac{T_{c,NOCT} - T_{a,NOCT}}{G_{t,NOCT}}\right)\left(1 - \frac{\eta_c}{0.9}\right)} \quad (8)$$

The average clearness index on a monthly basis is estimated using Eq. (9)

$$\boldsymbol{K_t = \frac{H_{avg}}{H_{0,avg}}} \quad (9)$$

Where: K_t is the Clearness index (ranging between 0 – 1), H_{avg} is the Average radiation on Earth's horizontal surface (kWh/m^2/day), and $H_{0,avg}$ is the radiation at the top of the earth's atmosphere on a horizontal plane (kWh/m^2/day).

3.1.2. Wind Turbine

The wind power calculation conducted by HOMER considers each time interval. In the first interval, the wind speed at the hub height of the turbine is estimated. The power produced by the turbine at a specific wind speed under a given air density is then calculated (Rai *et al.,* 2021). The power generated by a wind turbine can be calculated by Eq. (10) (Das *et al.,* 2017):

$$\boldsymbol{P_W = \begin{cases} 0, & V \le V_{Cut-in} \text{ and } \ge V_{Cut-out} \\ \frac{P_r (V - V_{Cut-in})}{V_r - V_{Cut-in}}, & V_{Cut-in} \le V < V_r \\ & P_r, V_r \le V < V_{Cut-out} \end{cases}} \quad (10)$$

Where: P_r is the rated power of the wind turbine (kW), V_r is the rated wind speed (m/s), $V_{Cut\text{-}in}$ is the cut in speed (m/s), $V_{Cut\text{-}out}$ is the furlong (or cut out) speed (m/s), and V is the wind speed at the desired height (m/s).
The wind speed, V (m/s) at the hub height, H (m) relies on the geographical location of the site and differs from that at the reference (or base) height. It is computed from Eq. (11) (Singh *et al.,* 2016):

$$\boldsymbol{V = V_{Base} \left(\frac{H}{H_{Base}}\right)^{\propto}} \quad (11)$$

Where: V is the Wind speed (m/s) at the desired height H (m), V_{Base} (m/s) is the wind speed at the base height, H_{Base} (m), α is a dimensionless power law coefficient, which accounts for the change in wind speed with height above the ground, and ranges between 0.1-0.4.

The power from the wind turbine power is estimated using Eq. (12) (Kumar and Rao, 2022):

$$\boldsymbol{P_{WTG} = \left(\frac{\rho}{\rho_0}\right) P_{WT,STP}} \quad (12)$$

P_{WTG} is the Power of the Wind Turbine Generator (kW), $P_{WT,STP}$ is the Power of the Wind Turbine at Standard Temperature and Pressure (i.e., standard conditions) (kW)

3.1.3. Diesel Generator (DG)

Whenever the battery storage of the HRES is unable to satisfy the load demand, the DG system is engaged as an additional power generation unit. The rating of the generator in HOMER Pro is computed using the "auto-size" function. The corresponding generator fuel consumption is estimated from Eq. (13) (Razmjooet *et al.,* 2019):

$$\boldsymbol{F = \left(F_{0,DG} \times Y_{DG}\right) + \left(F_{1,DG} \times P_{DG}\right)} \quad (13)$$

Where: $F_{0,DG}$ is the coefficient of fuel curve intercept (units/hr/kW), $F_{1,DG}$ is the gradient of the fuel curve (units/hr/kW), Y_{DG} is the rated capacity of the generator (kW); and P_{DG} is the power output of the generator (kW).

3.1.4. Biogas Generator (BG)

The daily power generated is given by Eq. (14) as follows (Viyaj, 2016; Zala and Jain, 2017):

$$\boldsymbol{P_{BIOG} = \frac{Q_{BIOG} \times CV_{BIOG} \times \eta_{BIOG}}{T_{OPD}}} \quad (14)$$

Where: P_{BIOG} is the power output from the biogas generator (kW), Q_{BIOG} is the quantity of biogas available (m^3). The average gas production from 1kg of fresh animal waste is taken as 0,04 m^3 of biogas. Therefore, Q_{BIOG} is obtained as 210 m^3 of biogas from the estimated 5.25 tonnes of collection per day. CV_{BIOG} is the calorific value of the biogas and ranges between 21-23MJ/m^3 (taken as 22MJ in this work). A conversion factor of 0.278 kWh per MJ of energy is taken to convert the assumed value into approximately 6 kWh. η_{BIOG} is the typical efficiency of the biogas generator and ranges between 25%-40% (taken as 32% in this work). T_{OPD} is the operational duration (h) (taken as 24 hrs in this work).

Substituting the values into Eq. (14), gives an approximate biogas generator output of 16.8 kW.

3.1.5. Battery

HOMER employs the kinetic battery model to calculate the energy drawn out or taken in by the battery storage (Khan *et al.,* 2022). The allowable maximum charging and discharging power

of the battery bank is obtained from Eq. (15) (Baneshi and Hadianfard, 2016):

$$\boldsymbol{P_{Batt,Cmax}} = \frac{\boldsymbol{min}\left(\boldsymbol{P_{Batt,Cmax,kbm}P_{Batt,Cmax,mcr}P_{Batt,Cmax,mcc}}\right)}{\boldsymbol{\eta_{Batt,C}}} \quad (\mathbf{15})$$

Where, $\eta_{Batt,c}$ is the efficiency of charge storage and is given by Eq. (16):

$$\boldsymbol{P_{Batt,Cmax,kbm}} = \frac{\boldsymbol{kQ_1e^{-k\Delta t} + Qkc\left(1 - e^{-k\Delta t}\right)}}{\boldsymbol{1 - e^{-k\Delta t} + c(k\Delta t - 1 + e^{-k\Delta t})}} \quad (\mathbf{16})$$

The power of storage charging that corresponds to the maximum charging rate is estimated using Eq. (17) as:

$$\boldsymbol{P_{Batt,Cmax,mcr}} = \frac{\left(\boldsymbol{1 - e^{-\alpha_c\Delta t}}\right)\left(\boldsymbol{Q_{max} - Q}\right)}{\boldsymbol{\Delta t}} \quad (\mathbf{17})$$

The power of storage charging that corresponds to the maximum charging current is estimated using Eq. (18) as:

$$\boldsymbol{P_{Batt,Cmax,mcc}} = \frac{\boldsymbol{N_{Batt} \times I_{max} \times V_{nom}}}{\boldsymbol{1000}} \quad (18)$$

Where: k is the Constant for the storage rate (h^{-1}), $Q1$ is the SOC during the initial time step (kWh), $\Delta\boldsymbol{t}$ is the Time step duration (h), Q is the total amount of energy in the battery at any time (kWh), c is the capacity ratio of the battery, α_c is the maximum charging rate of the battery (A/Ah), N_{Batt} is the number of batteries, I_{max} is the peak charging current of the battery (A) and V_{nom} is the nominal voltage of the battery (V)

3.1.6. Bi-directional converter

The converter is sized to an appropriate power capacity to connect the AC and DC buses and inter-conversion from DC to AC. The converter functions as a power conditioning unit and sustains the power flow in the HRES. The efficiency of the converter is calculated from Eq. (19) (Khan *et al.,* 2022):

$$\boldsymbol{\eta_{in}} = \frac{\boldsymbol{P_o}}{\boldsymbol{P_{in}}} \quad (19)$$

Where: $\boldsymbol{\eta_{in}}$ is the Inverter Efficiency, $\boldsymbol{P_o}$is the Power output from inverter, and $\boldsymbol{P_{in}}$ is the Power input into the inverter

For this work, the converter size is taken as 10% greater than the peak load.

3.1.7. Justification of Critical Assumptions

Battery Charging Efficiency

The round-trip charging efficiency for each battery type was obtained from manufacturer datasheets and peer-reviewed literature. For lead-acid batteries, a value of 85% was adopted (Baneshi & Hadianfard, 2016; Khan *et al.,* 2022), consistent with both HOMER Pro default settings and experimental results from similar rural off-grid applications. For lead-carbon batteries, a slightly higher efficiency of 88% was assumed, reflecting improved charge acceptance reported in recent studies (Mala & Saini, 2020). Lithium-ion batteries were assigned a 95% efficiency, based on published specifications for $LiFePO_4$-based modules suitable for off-grid use (Bhatt *et al.,* 2022). These values were cross-checked against HOMER defaults to ensure internal consistency.

PV Derating Factor

A derating factor of 90% was applied to account for combined system losses due to wiring, dust accumulation, temperature effects, and minor shading. This value was selected based on National Renewable Energy Laboratory (NREL, 2019) guidelines and field measurements in sub-Saharan Africa, where soiling and high ambient temperatures are common (Micangeli *et al.,* 2017). A ±5% variation in this factor was tested to confirm that results were robust, with less than 3% impact on LCOE.

Biogas Yield Estimates

The biogas yield from livestock manure was calculated using an average production rate of 0.04 m^3/kg of fresh waste, consistent with values reported in Werner *et al.* (1989) and Mwakitalima *et al.* (2023) for cattle, goats, pigs, and poultry manure under mesophilic digestion. The calorific value was taken as 22 MJ/m^3, aligned with standard literature values (Zala and Jain, 2017). A collection efficiency of 60% was assumed due to the free-grazing nature of livestock in the area. This figure was obtained from the Zambian Ministry of Livestock and Fisheries.

3.1.8. Pollutant emissions

HOMER calculates the emissions resulting from running the diesel generator. In particular, emissions in the form of carbon dioxide (CO_2), carbon monoxide (CO), unburned hydrocarbons (UHC), particulate matter (PM), Sulphur dioxide (SO_2) and nitrogen oxides (NO_x), are calculated by determining the emission factor for each pollutant (kg of pollutant emitted per unit of fuel consumed). This factor is multiplied by the total annual fuel consumption to get the annual emissions of the respective pollutant HOMER Pro 3.14 User Manual, (2020).

3.2. HRES Economics

The economic parameters used to appraise the feasibility of the designed HRES are the COE and NPC.

3.2.1. Cost of Energy (COE)

The COE is calculated from Eq. (20) (Li *et al.,* 2022):

$$\boldsymbol{COE} = \frac{\boldsymbol{Cann,tot}}{\boldsymbol{E_{Served}}} \quad (20)$$

Where:

$$\boldsymbol{C_{ann,tot}} = \boldsymbol{CRF}\left(\boldsymbol{i \times R_{Proj}}\right)\boldsymbol{C_{NPC}} \quad (21)$$

Where:

$$\boldsymbol{CRF} = \frac{\boldsymbol{i(1+i)^N}}{\boldsymbol{(1+i)^N - 1}} \quad (22)$$

Where: E_{served} is the total electrical energy served in a year (kWh/yr), $C_{ann.tot}$ is the total cost of the HRES in a year (USD/yr), CRF is the Capital Recovery Factor, i is the real discount rate, N is the number of years, C_{NPC} is the Net Present Cost and R_{Proj} is the project lifetime.

3.2.2. Net Present Cost (NPV)

The NPC of the HRES is essentially the today's value of all capital and O&M costs over the project life minus the present value of all the income that the system earns over the project ifetime (Ramesh and Saini, 2020).

3.3. Techno-Economic Specifications of the HRES components

This study considered three types of solar PV panels, rated at 335 W, 400 W and 445 W, one wind turbine, rated at 1 kW, three types of batteries namely 100 Ah LA, 200 Ah LC, and 100 Ah Li- ion, and a converter rated at 344 kW. The specifications of the main components that were considered as inputs into HOMER are presented in Table 2.

To ensure realistic operation, the following constraints were applied in HOMER Pro during optimization: Maximum annual capacity shortage is limited to 0% of the total annual load to guarantee supply reliability; Minimum State of Charge (SoC) for batteries is fixed at 10%, 20% and 20% for Li-Ion, LA and LC respectively, to preserve battery health and extend storage life; Minimum and maximum renewable penetration is capped at 55% and 100% respectively, to ensure grid stability and avoid excessive curtailment; Dispatch strategies, Predictive Dispatch (PD), Cycle Charging (CC) or Load Following (LF) are chosen to balance fuel consumption and battery cycling; Project lifetime and component replacement limits are defined to reflect realistic system durability and cost recovery as indicated in Table 2.

3.4. Dispatch strategies

For enhanced system performance, the HRES system design requires an effective Dispatch Strategy (DS). The DS consists of a code that governs and operates the generators and storage batteries whenever the power from renewable energy is

Table 2
Input specifications of HRES components

Component	Model	Manufacturer	Rating	Voltage	Capital Cost (USD)	Replacement Cost (USD)	O&M Cost (USD)	Lifetime	Notes*
Solar PV	AS-335	Dayliff	335 W	12 V	883	490	8.83	25 years	Derating: 88% Ground reflection: 88%
	TL-400M	Suntech	400 W	12 V	997	554	9.97	25 years	Derating: 88%
	JAM-72S20	Dayliff	445 W	12 V	728	404	7.28	25 years	Ground reflection: 88%
Wind Turbine	HY-CI10-48-AWMMT	Kirloskar	1 kW	48 V	13,377 (per unit)	8,360	133	20 years	Hub height: 17 m
Diesel Generator	Generic 350 kW	Dayliff	350 kW		516	287	0.030 /op.hr	60,000 hours	Fuel: Diesel Fuel cost: USD 1.30/L
Biogas Generator	Generic	Dayliff	16.8 kW		550	450	0.10 /op.hr	20,000 hours	Fuel: Biogas
Battery - Lead-Acid	4R-1040TC	Rentech	1.2 kWh	12 V	1092 (set of 4)	840 (set of 4)	1.09 (set of 4)	5 years	Max capacity: 100 Ah
Battery - Lead-Carbon	NP-100-12 L	WECO	2.63 kWh	12 V	2527 (set of 4)	1944 (set of 4)	2.53 (set of 4)	15 years	Max capacity: 200 Ah
Battery - Lithium-Ion	JPC 12-200	WECO	5.2 kWh	48 V	3275 (per unit)	2519 (per unit)	3.30 (per unit)	15 years	Max capacity: 100 Ah
Converter	Generic		344 kW						Efficiency: 95%

unable to satisfy the load demand. The five main DS codes found in HOMER are Load Following, Cycle Charging, Combined Dispatch -, Generator Order (GO), Predictive Dispatch (PD), Intra-Time-Step Distribution (ITS) and Matlab Link (ML) (Kushwaha and Bhattacharjee, 2022). The four strategies that are considered for study are Load Following, Cycle Charging, Combined Dispatch and Predictive Dispatch.

Table 3:
Comparative studies on NPC and COE results for Zambia and parts of Sub-Saharan Africa

Authors	HRES Configuration(s) investigated	Region & Peak Load	Technique / Tool	Battery Type & Dispatch Strategy	Objective Function	Findings
Present Work	PV/WT/DG/BT, PV/DG/BT, PV/BG/BT and PV/BT	Chinyunyu, Zambia, 312kW	HOMER	BT: LA, LC, Li-Ion DS: LF, CC, CD, PD	NPC = $3,886,892 COE = $0.1522/kW	The PV/DG/BT combination is found to be the most cost-effective when using larger-sized PV panels along with the Li-Ion battery under the PD Strategy.
Araoye et al. (2023)	PV/DG/BG/BT	Enugu State, Nigeria, 104.1kW	HOMER	BT: Li-Ion DS: Not Stated	NPC = $303,312 COE = $0.066	Increasing the proportion of biogas in the HRES eventually eliminates the need for DG and reduces the NPC and COE.
Chisale et al. (2023)	DG/Grid, PV/DG/Grid PV/BG/Grid PV/WT/BG/Grid BG/Grid , PV/BT/Grid	Blantyre, Malawi, 23.7kW	HOMER	BT: Not Stated DS: Not Stated	NPC = $79,511 COE = $0.095/kWh	The PV/BG/Grid system is found to be the most cost-effective. The addition of DG increases NPC values, while the inclusion of batteries increases the operating costs due to their short life span.
Kapole et al. (2023)	PV/BT	Various locations in Zambia, 24.4 – 51.8kW	End use model, basic financial equations.	BT: Not Stated DS: Not Stated	COE = 0.4 – 0.57kWh	PV mini-grids in rural areas are generally not economically viable and may need an element of subsidy.
Mwakitalima et al. (2023)	PV/BG/BT	Mbeya, Tanzania 63.41kW	HOMER, GWO	BT: Li-Ion DS: Not Stated	NPC = $106,383.50 COE = $0.1109/kWh NPC = $85,106, COE = $0.0887/kWh	The application of the GWO technique shows a decline in financial metrics.
Samikannu et al. (2022)	PV/WT/BT	Jamataka, Botswana, 27.31kW	HOMER	BT: LA DS: Not Stated	NPC = $339,804 COE = $0.298/kWh	The Capacity of battery systems must be carefully considered along with their O&M costs during the design stage of HRES
Perez et al. (2021)	PV/BM/BT	El Santuario, Honduras. 8kW Mumbezi, Zambia, 0.5kW	HOMER	BT: Not Stated DS: Not Stated	NPC = $256,133 COE = $0.06/kWh NPC = $564,697, COE = 0.48/kWh	Technical and Economic aspects of islanded PV-biomass hybrid microgrid are found viable as compared to grid extension in both cases.
Oloo et al. (2020)	PV/WT/DG/BT	Eastern Cape, South Africa, 54.34	HOMER	BT: Li-Ion DS: LF, CC, CD, PD	COE = $0.1382/kWh	PD strategy found to be the most optimal.

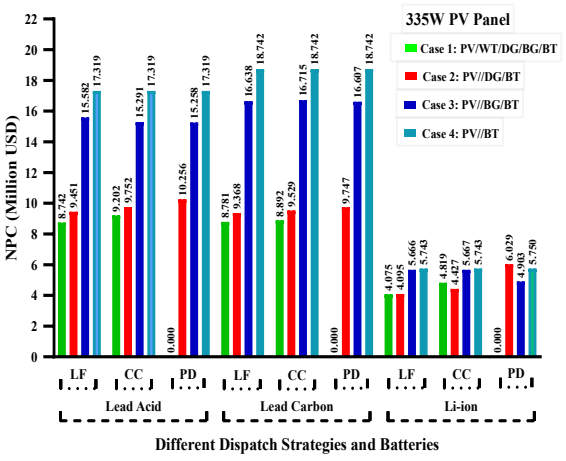

Fig. 6a: NPCs with 335W PV Panel

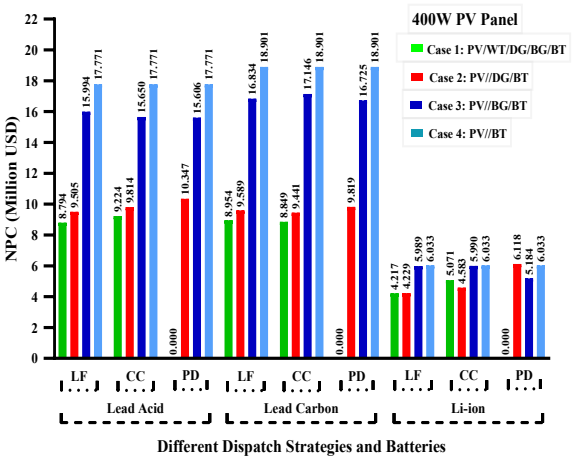

Fig. 6b: NPCs with 400W PV Panel

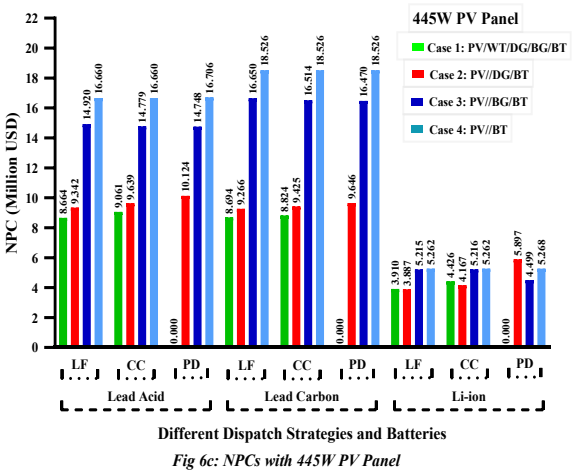

Fig 6c: NPCs with 445W PV Panel

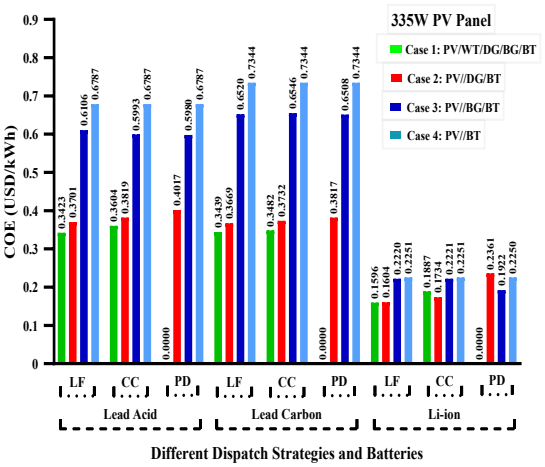

Fig. 6d: COEs with 335W PV Panel

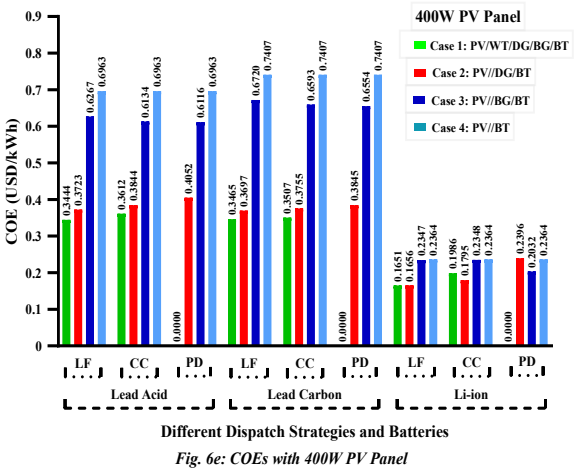

Fig. 6e: COEs with 400W PV Panel

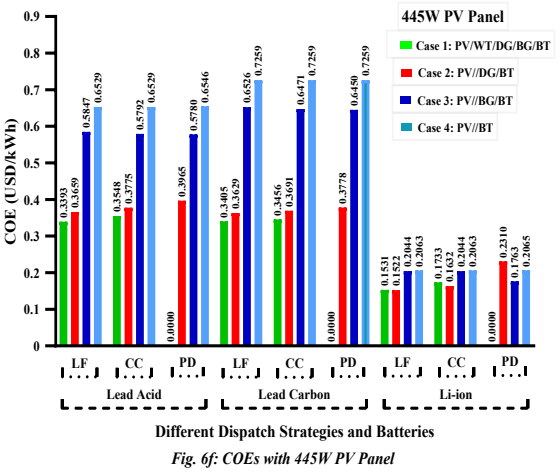

Fig. 6f: COEs with 445W PV Panel

Fig. 6 The NPC and COEs obtained for the four HRES configurations considered.

The LF strategy code switches on the generator to deliver sufficient power to fulfill the demand, whilst energizing the battery by using the renewable energy sources (Fofang and Tanyi, 2020). In the CC strategy, the generators run at maximum capacity primarily to meet the load, and thereafter using the surplus power (if available) for energizing the batteries (Kumar, 2022). The CD strategy code by-passes upcoming load estimation and uses the existing load to assess on whether or not to use the generator to energize the battery. Within the CD strategy, the CC strategy is utilized for low load, and LF is used for high load to aid in reducing the operating costs of the HRES. In the PD strategy code, the upcoming load and resources such as solar radiation and wind speed are "predicted" to help in reducing the HRES cost through cost-effective discharging of the batteries.

3.5. Multi-Criteria Decision Analysis (MCDA)

To integrate both economic and environmental performance into a single decision framework, a simple Multi-Criteria Decision Analysis (MCDA) approach was applied. The MCDA enables identification of the preferred Hybrid Renewable Energy System (HRES) configuration when decision priorities

vary between cost minimization and emissions reduction. To combine economic and environmental performance into a single decision framework, NPC and annual CO_2 emissions were selected as the evaluation metrics. Using Eq. (23), both metrics were normalized to a 0–1 scale using min–max scaling, with higher scores representing better performance (lower cost or lower emissions).

$$S_{i,j} = \frac{max(x_j) - x_{ij}}{max(x_j) - min(x_j)} \quad (23)$$

Where: S_{ij} is the normalized score for option *i (systems design)* on criterion *j* (economic cost and environmental impact) scaled to [0,1], $max(x_j)$ is maximum value for criterion *j* across all options, $min(x_j)$ is the minimum value observed for criterion *j* across all options, and x_{ij} is the performance of option i (system design) on criterion *j*. For cost metrics (NPC), lower values correspond to higher normalized scores, while for emissions, lower emissions correspond to higher scores.

Three weighting schemes were applied: cost-centric (70% cost, 30% emissions), balanced (50% cost, 50% emissions), and environment-centric (30% cost, 70% emissions). For each configuration, a weighted score was calculated by multiplying the normalized cost and emissions scores by their respective weights and summing the results using Eq. (24).

$$\text{Weighted Score}_i = \left(w_{cost} \times \text{Score}_{cost,i}\right) + \left(w_{emissions} \times \text{Score}_{emissions,i}\right) \quad (24)$$

Where w_{cost} and $w_{emissions}$ are the assigned weights for cost and emissions, respectively.

The configurations were ranked under each weighting scheme to identify how the optimal choice shifts when priorities change. Cost-centric weights favor the lowest-cost system, environment-centric weights favor the lowest-emissions system, and balanced weights select a compromise between the two.

4. Results and Discussion

The performance analysis of the PV/WT/DG/BG/BT-based HRES being proposed is conducted by considering different ratings of PV panels, different dispatch strategies (LF, CC, CD, and PD), and different types of batteries (LA, LC, and Li-ion). The HRES performance is further analyzed in reference to pollutant emissions and sensitivity. The NPC and COE are found to be USD 14,101,860 and USD 0.5523, respectively, for the base case. The results obtained in this study are found to be comparable to those reported from case studies for similar rural electrification projects carried out in other parts of Zambia and Sub-Saharan Africa as summarized in Table 3.

4.1. Techno-economic analysis with respect to PV panels

The techno-economic analysis of the proposed HRES is evaluated by considering three different ratings of PV panels, viz., 335, 400, and 445 W. The obtained NPC and COE of the HRES using three different ratings of PV panels, battery technologies, and four different dispatch strategies, are given in Fig 6(a-f). For the 335 W and 400 W PV panels, the lowest NPC values under the load-following (LF) strategy are observed in Case-1 (PV/WT/DG/BIOG/BT), indicating that a diversified mix of renewables with storage provides the most cost-effective option at lower PV capacities. However, when the 445 W PV panel is considered, the trend changes: Case-2 (PV/DG/BT) emerges as the most economical, highlighting that higher-capacity PV modules reduce the reliance on additional renewable components, making a simpler configuration more favorable. This demonstrates that the choice of optimal configuration is sensitive to PV panel capacity, with larger modules shifting the balance toward leaner system designs. The results show that the NPC is maximum when the lead-carbon type battery is used under the cycle charging (CC) strategy. Furthermore, it has been noted that the 400 W PV panel offers the highest NPC whereas the 335 W PV panel yields lower NPC. When compared to the 335 W and 400 W PV panels, it is evident that the 445 W PV panel provides the best outcomes. For example, using a 400 W PV panel and an LC battery under the CC strategy in Case-4, the NPC value is found to be 34 % more than the base case. However, using the 335 W PV panel, the NPC is found to be 32 % more than the base case. Further, when using the 445 W PV panel, it is seen that the NPC is only about 31 % more than the base case. These values happen to be the maximum amongst the NPC values obtained from all the combinations. When using Li-ion battery under LF strategy for Case-2, the NPC is about 70% less than the base case using 400 W PV panel whereas, for the 335 W PV panel, the NPC is about 71 % less than the base case. However, with the 445 W PV panel the optimal NPC is obtained and about 72 % less than the base case. From the three different PV panel ratings, it is found that the 445 W PV panel turned out to be the most cost effective. Hence, further analysis of the HRES will be discussed with respect to 445 W PV panel only.

In order to monitor the power sharing between different components of the system, the curves of output power for the base case, PV/WT/DG/BG/BT, PV/DG/BT/, PV/BG/BT and PV/BT whilst utilizing the Li-ion battery type under the LF strategy for a typical week from 1st December to 7th December are shown in Fig. 7(a-e). Fig. 7a shows that the power demand is met by the diesel generator, Fig. 7b shows that the load demand is met by PV/WT/DG/BG/BT HRES which consists of all the system components which are considered. Whenever solar radiation is available, the major portion of load demand is met by PV panels. However, the Biogas generator delivers a constant power output of 16.8 kW, while the wind generator contributes a 1 kW power output. The batteries discharge power when renewable energy resources are unavailable, typically during the night when solar energy, the dominant resource, is absent. During this period, if the SoC of the battery is less than 10 %, the DG is turned on. Fig 7c shows that in the PV/DG/BT configuration, the battery and DG deliver power similarly to Fig 7b. Fig. 7d reveals that in the PV/BG/BT configuration, the BG delivers 16.8 kW, which is insufficient to meet the peak demand. Consequently, the load must be supplied by the PV system and batteries. This results in an increase in the NPC and COE by about 25% compared to the PV/WT/DG/BG/BT configuration. From Fig. 7e, it is observed that the load demand must be met entirely by the PV system and batteries. The increase in NPC and COEs is the same as Fig. 7d. The curves show that apart from the base case, during sunshine hours, the electric load demand is mainly met by the PV system, which also energizes the battery bank. At night, the battery, wind turbine, and generator cater to the demand. It is also seen that the demand is first met by the battery bank and that both the diesel and biogas generators only "kick in" during the early hours of the morning or during periods of low solar radiation or low clearness index, when the batteries discharge below the predefined 10% limit.

4.2. Effect of different strategies on HRES Performance

To evaluate the effect of LF, CC, CD and PD strategies on the functioning of HRES, four distinct configurations (Case-1, Case-

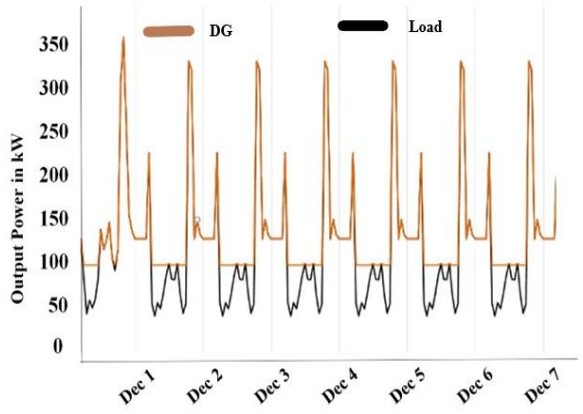

Fig. 7a Power output curve for the base case (DG only

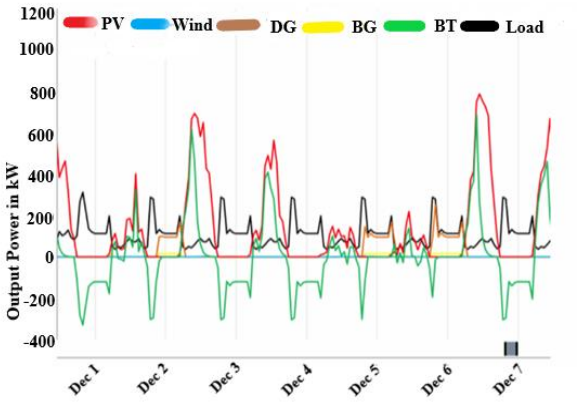

Fig. 7b Power output curve for the PV/WT/BG/DG/BT HRES

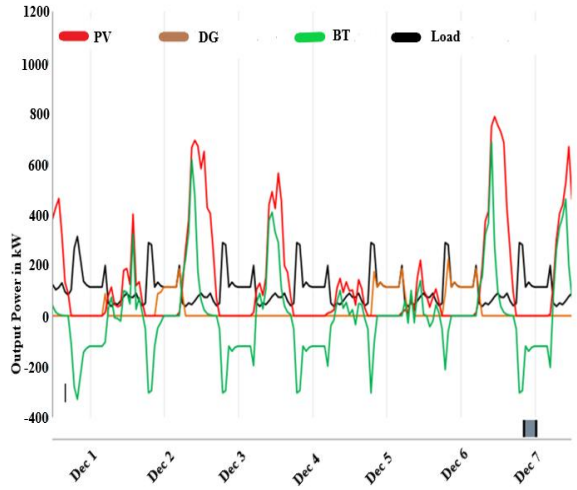

Fig. 7c Power output curve for the PV/DG/BT HRES

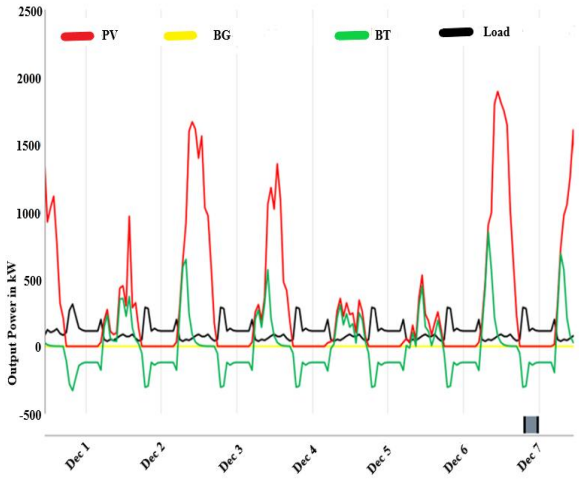

Fig. 7d Power output curve for the PV/BG/BT HRES

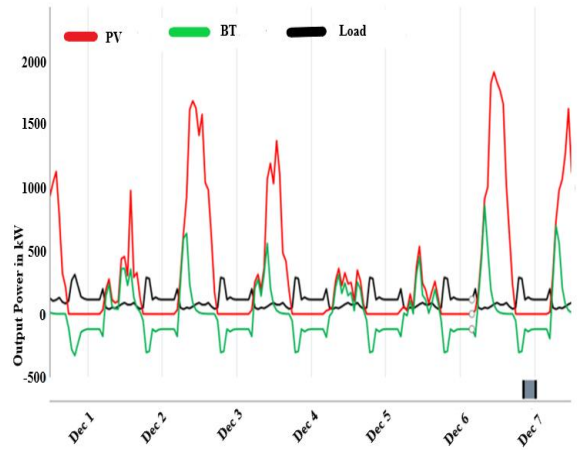

Fig. 7e Power output curve for the PV/BT HRES

Fig. 7. Power output curves for the four HRES configurations considered for the period 1st December to 7th December

2, Case-3, and Case-4) have been considered. Out of them, the PV/DG/BT (Case-2) is found to be the optimal configuration. The NPC and COE parameters under the PV/WT/DG/BG/BT (Case-1) configuration are found about 0.6 % higher than those of the optimal configuration. This difference is not significant, especially when data uncertainties are taken into account. However, under PV/BT (Case-4) configuration, these parameters are found greater than the base case (DG only). Under CC strategy, the NPC is about 70 % less than the base case, and about 68 % under PD strategy. However, under the LF strategy, it is about 72 % less than the base case. As the CD strategy performs with only one generator, it will not give any results. The same trend is seen as COEs under different dispatch strategies. Hence, it is found that the LF strategy offers the most optimal option among other dispatch strategies. Table 4 shows the optimized results for the four selected cases PV/WT/DG/BG/BT (Case-1), PV/DG/BT (Case-2), PV/BG/BT (Case-3) and PV/BT (Case 4).

4.3. Effect of batteries on HRES performance

When designing battery storage-based systems, it is important to ensure that the battery SoC remains within pre-defined limits (Singh *et al.,* 2016). Therefore, to evaluate the

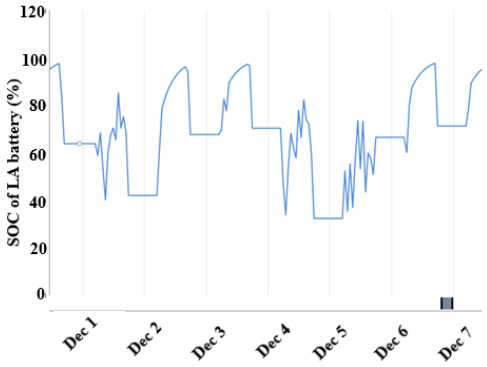

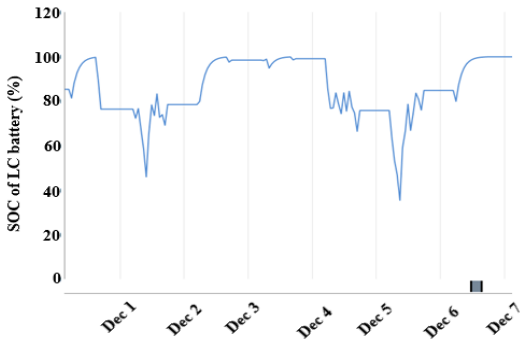

Fig. 8b SoC of LC battery in a week

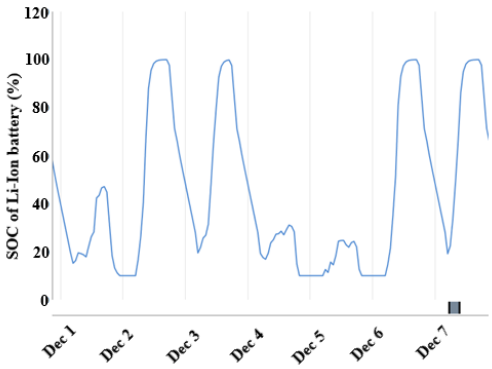

Fig. 8c: SoC of Li-ion battery in a week

Fig. 8. Weekly State of Charge (SoC) of the three battery types

effect of batteries on the proposed HRES performance, the three different batteries have been considered viz: LA, LC and Li-ion. The SoCs of these batteries for a typical week (1st December to 7th December) have been shown in Fig. 8a, 8b and 8c. From Fig. 8a, it can be seen that LA battery is discharged to nearly 36 % for the chosen week, whereas, the LC battery discharged down to 38 % in that week. However, the Li-ion battery is discharged to a much deeper extent, with only about 10% of its charge remaining. This indicates a depth of discharge (DoD) of approximately 90%, which is significantly higher than the DoD observed for the LA (36%) and LC (38%) batteries during the chosen week. While the DoD limits for these batteries are provided by the manufacturers, the observed behavior in this study demonstrates that Li-ion batteries can operate closer to their maximum DoD under the given conditions. This higher usable capacity allows Li-ion batteries to supply power for a longer period, reducing the frequency of recharging cycles. Additionally, the superior energy density and efficiency of Li-ion batteries mean that fewer batteries are required to meet the same energy demand, which directly contributes to a reduction in the present net cost (NPC) of the system. These advantages make Li-ion batteries a more cost-effective and reliable option for the hybrid renewable energy system (HRES) under study.

From Figs. 8a, 8b and 8c, it is evident that the depth of discharge (DoD) varies across the three battery types. For the selected week (1st–7th December), the Lead-Acid (LA) battery is discharged down to approximately 36% State of Charge (SoC) corresponding to a DoD of about 64%. Similarly, the Lead-Carbon (LC) battery is discharged to around 38% SoC (DoD ~62%).

In contrast, the Li-ion battery is discharged much deeper, exhibiting a DoD of approximately 90% (maintaining a minimum SoC of only ~10%).

This significantly higher DoD observed for Li-ion batteries enables greater usable capacity per cycle, allowing them to meet higher energy demands with fewer units. Additionally, their superior energy density, efficiency, and longer lifespan contribute to reduced system size and frequency of replacement. These factors collectively result in a lower Net Present Cost (NPC) and make Li-ion batteries a more cost-effective and reliable choice for the hybrid renewable energy system (HRES) evaluated in this study.

Fig. 9 shows the SoC of the Li-ion battery in a year, in a month and in a day. From Fig. 9a, it is observed that from December to March, the batteries are discharging up to 10 %. The reason for this is the low clearness index (reduced solar radiation) during rainy season and higher load demand primarily from lighting. The slow charging rate during this period further exacerbates the discharge. From April to August, it is seen that the batteries are discharging to around 30 %, reflecting a higher clearness index and lower load demand during the cool dry season. However, during Summer season from September to November, the batteries discharge again to 10 %. This is due to the higher usage of fans that leads to high load demand despite the higher clearness index. Fig. 9b provides a clearer view of the battery discharge pattern during the rainy season, particularly in December. Fig. 9c highlights the daily behaviour. During the night, the load demand relies heavily on the batteries, causing discharge to around 20 %. Soon after solar radiation picks-up, the majority of the load demand is met by PV panels, and the batteries begin charging, reaching the maximum state of charge (SoC_{Max}).

From Fig. 6, it is found that by using LC batteries, the NPC and COEs are the highest as compared to the values obtained using other two battery types. However, using the Li-ion battery, the NPC and COEs are found to be the most cost

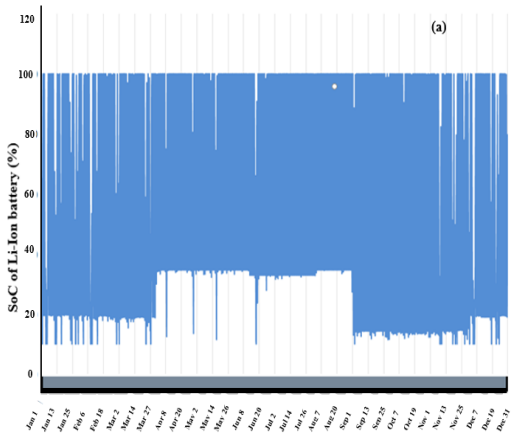

Fig 9a: Yearly SoC of the Li-ion battery

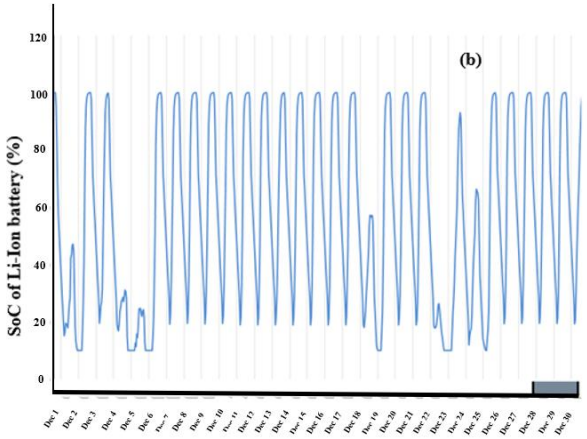

Fig 9b: Monthly SoC of the Li-ion battery

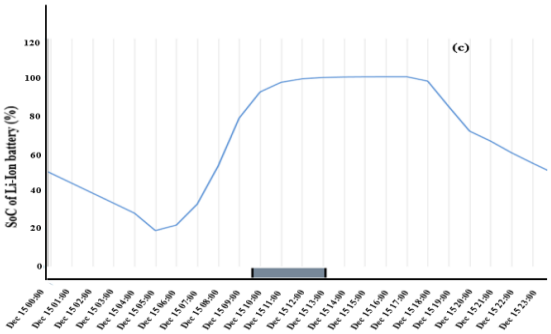

Fig 9c: Daily SoC of the Li-ion battery

Fig. 9. State of Charge (SoC) of the Li-ion battery over different time periods

effective. In addition, it is observed that from the four different configurations, Case-1 offers the least costs when using the LA and LC batteries, whereas Case-2 offers the least costs when using the Li-ion battery. When the NPCs are compared to the base case, it is found that there is a reduction in NPC of about 33 % and 34 %with LA and LC batteries respectively. However, by using Li-ion battery, it is observed that there is a huge reduction in NPC of about 72 % from the base case. The

Table 4
Optimization results of 445W based HRES under different strategies and batteries

Dispatch Strategy	Load Following (LF)											
Battery Type	Lead Acid				Lead Carbon				Li-ion			
Case No	1	2	3	4	1	2	3	4	1	2	3	4
PV (kW)	365	552	2,732	3,055	510	504	1,443	1,092	1.021	1,017	2,449	2,478
Wind (Nos.)	1				3	-		-	3	-	-	-
DG (kW)	350	350			350	350			350	350	350	-
BG (kW)	16.8	-	16.8	-	16.8		16.8		16.8		16.8	
Battery (Nos.)	178	178	2,436	2,766	116	136	1,690	2,450	438	439	530	534
Converter (kW)	344	344	344	344	344	344	344	344	344	344	344	344
Dispatch Strategy	Cycle Charging (CC)											
Battery Type		Lead Acid				Lead Carbon				Li-ion		
Case No	1	2	3	4	1	2	3	4	1	2	3	4
PV (kW)	566	547	2,488	3,055	485	585	769	1,092	1,847	1,326	2,449	2,478
Wind (Nos.)	1	-	-	-	5	-	2	-	1	-	1	-
DG (kW)	350	350	350		350	350	-	350	350	350		350
BG (kW)	16.8		16.8		16.8		16.8		16.8		16.8	
Battery (Nos.)	130	164	2,448	2,766	118	124	2,452	2,450	444	445	530	534
Converter (kW)	344	344	344	344	344	344	344	344	344	344	344	344
Dispatch Strategy	Predictive Dispatch (PD)											
Battery Type		Lead Acid				Li-ion				Lead Acid		
Case No	1	2	3	4	1	2	3	4	1	2	3	4
PV (kW)	-	790	2,448	3,105	-	494	790	1,092	-	700	1,938	2,484
Wind (Nos.)	-	-	-	-	-	-	-	-	-	-	-	-
DG (kW)	-	350	-	-	-	350		-	-	350		-
BG (kW)	-	-	16.8		-		16.8		-		16.8	
Battery (Nos.)	-	140	2,460	2,760	-	346	2,410	2,450	-	207	481	534
Converter (kW)	-	344	344	344	-	344	344	344	-	344	344	344

**The PD Strategy does not yield any results for Case 1; The CD Strategy yields no results*

performance of LA, LC and Li-ion batteries for the four cases under the LF strategy is presented in Table 4. It is observed that using Li-ion batteries results in a greater lifetime throughput compared to the other two battery types. The losses from the Li-ion battery type are also observed to be, on average, lower than the LA and LC types of batteries, especially for Cases 3 and 4, where the system is more dependent on the battery.

4.4. Impact of dispatch strategies on pollutant emissions

As shown in Table 5, in the base case, where only the diesel generator (DG) provides the load demand, the annual CO_2 emissions are estimated to be 793,467 kg/year, including significant emissions of other pollutants: 5,002 kg/year of CO, 218 kg/year of UHC, 30.3 kg/year of PM, 1,943 kg/year of SO_2, and 4,698 kg/year of NOx. These pollutants contribute to air pollution, health issues, and environmental degradation.

However, when the proposed HRES supplies the load, emissions are drastically reduced across all pollutants. For instance, under the Load Following (LF) strategy in Case 3, CO_2 emissions are reduced to 0.0778 kg/year, representing a 99.9 % reduction compared to the base case. Similarly, other pollutants are reduced to close to zero levels, i.e., 0.000864 kg/year of CO, 0 kg/year of UHC, 0 kg/year of PM, 0 kg/year of SO_2, and 0.000540 kg/year of NOx. This reveals the environmental superiority of the HRES over the DG-only system.

The quantity of emissions depends heavily on the dispatch strategy employed. For instance, under the Predictive Dispatch (PD) strategy in Case 2, CO_2 emissions are 375,330 kg/year, significantly higher than those under the LF strategy but still represent a 52.7 % reduction compared to the base case. Other pollutants under the PD strategy in Case 2 are also reduced but remain higher than in the LF strategy: 2,366 kg/year of CO, 103 kg/year of UHC, 14.3 kg/year of PM, 919 kg/year of SO2, and 2,222 kg/year of NOx. This highlights the tradeoff between dispatch strategies, with the LF strategy achieving the lowest emissions. Among the dispatch strategies, the LF strategy in Case 3 emerges as the most effective in reducing emissions, achieving nearly 100% reduction for most pollutants. Comparing this to the PD strategy in Case 2, there is a 47.2% difference in emissions reduction, further emphasizing the environmental benefits of the LF strategy. Given that the optimization of net present cost (NPC) and cost of energy (COE) is the primary objective of this study, the LF strategy is recommended for the HRES. It not only aligns with the economic goals but also ensures minimal environmental impact by reducing pollutant emissions to almost negligible levels. This makes it a more sustainable and environmentally friendly choice compared to the PD strategy.

4.5. Trade-off Analysis between Economic and Environmental Performance

The normalized scores for cost (NPC) and CO_2 emissions were combined using the three weighting schemes specified in the methodology: cost-centric (70% cost, 30% emissions), balanced (50% cost, 50% emissions), and environment-centric (30% cost, 70% emissions). Table 6 reports the weighted scores and rankings. The configuration with the highest weighted score under a given scheme is considered the preferred option for that priority setting.

Under the cost-centric scheme (0.7/0.3), Case 1 (PV/WT/DG/BG/BT) attains the highest score (0.724), narrowly outperforming Case 2 (0.700). Although Case 2 has the lowest NPC, the small cost advantage over Case 1 is offset by Case 1's substantially lower emissions; with a 30% weight on emissions, this difference is decisive. With balanced weights (0.5/0.5), Case 1 again ranks first (0.549), followed by Case 3 (0.515). Cases 2 and 4 tie (0.500). The result reflects Case 1's combination of very low cost and materially better emissions than Case 2. Under the environment-centric scheme (0.3/0.7), Case 3 (PV/BG/BT) ranks first (0.709), closely followed by Case 4 (PV/BT) (0.700), both achieving near-zero emissions; Case 3's slightly better cost yields the edge. Case 1 is third and Case 2 fourth because of their higher emissions.

Overall, the preferred configuration shifts with stakeholder priorities: a cost-leaning or balanced focus favors the diversified PV/WT/DG/BG/BT (Case 1), whereas an emissions-dominant focus favors PV/BG/BT (Case 3).

4.6. Sensitivity Analysis

A sensitivity analysis was conducted by varying the discount rate, PV cost, battery cost, and fuel cost, and studying the effect upon NPC, COE, and load demand under Zambian conditions. The economic and cost data for this case were collected from

Table 5
Details of pollutant emissions under different strategies

	Dispatch Strategies								
	Base Case	Load Following (LF)			Cycle Charging (CC)			Predictive Dispatch (PD)	
Emissions (kg/yr)	DG Only	Case 1	Case 2	Case 3	Case 1	Case 2	Case 3	Case 2	Case 3
CO_2	793,467	21,182	23,882	0.0778	9,047	2,460	0.205	375,330	2.38
CO	5,002	134	151	0.000864	57	155	0.00228	2,366	0.0264
UHC	218	5.83	6.57	0	2.49	6.77	0	103	0
PM	30.3	0.809	0.912	0	0.346	0.941	0	14.3	0
SO_2	1,943	51.9	58.5	0	22.2	60.3	0	919	0
NOx	4,698	125	141	0.000540	53.6	146	0.00142	2,222	0.0165

Table 6
Weighted scores and rankings for each HRES configuration

Case	Config	NPC (USD M)	CO_2 (kg/yr)	Norm. Cost	Norm. CO_2	Cost-Centric (0.7/0.3)	Balanced (0.5/0.5)	Env.-Centric (0.3/0.7)	Rank C-C	Rank Bal	Rank Env
1	PV/WT/DG/BG/BT	3.91	21,182	0.985	0.113	0.724	0.549	0.375	1	1	3
2	PV/DG/BT	3.89	23,882	1.000	0.000	0.700	0.500	0.300	2	3	4
3	PV/BG/BT	5.22	0.078	0.029	1.000	0.320	0.515	0.709	3	2	1
4	PV/BT	5.26	0.000	0.000	1.000	0.300	0.500	0.700	4	3	2

local suppliers. To validate the results, a further analysis was conducted using economic and cost data for the African region, obtained from IEP (2024) and IRENA-RPGC (2025). For this case, due to the vast range in the data sets, the median of the respective ranges was considered to study the variations. In both cases, the economic and cost data were varied by ±20%.

4.6.1. Effect of Change in Input Economic Parameters on NPC

The input parameters—discount rate, PV cost, battery cost, and fuel cost—were varied by ±20%, and their effects on the Net Present Cost (NPC) and Cost of energy (COE) are illustrated in Fig. 10 for Zambian and African regions respectively. The results show that the NPC varies approximately in direct proportion to the input changes. Among the parameters tested, fuel cost has the least effect, resulting in only a ±0.81–1.81% change in NPC for Zambian conditions and ±0.81-2.07% for regional conditions. and. A ±20% change in PV cost leads to a relatively larger but still low impact, with a ±2.25–5.07% change in NPC for Zambian conditions and ±2.32 and 4.97% for regional conditions. Meanwhile, battery cost has the greatest influence among the parameters, with a ±5.48–11.78% variation in NPC for Zambian conditions and ±5.36 % and 11.32% for regional conditions.

The relatively low sensitivity of NPC to fuel cost can be attributed to the operational characteristics of the Load-Following (LF) dispatch strategy. In this strategy, the diesel generator is primarily used when renewable sources are insufficient, and renewable energy is prioritized for charging batteries. As a result, fuel consumption is relatively low, and so is the system's sensitivity to fuel price variations.

The significant impact of battery cost on NPC highlights the crucial role of battery technology advancements and economies of scale in improving the economic feasibility of HRES. Although the sensitivity analysis indicates that reductions in battery costs can lower the NPC, the extent to which this shift would make the entire system substantially more economically feasible would require further detailed analysis beyond the scope of the current study. Nevertheless, it suggests that battery cost reductions are a promising area for future improvement.

Conversely, the relatively lower sensitivity to PV cost indicates that while solar panels are important, their contribution is limited by the inherent intermittency of solar energy availability, which necessitates greater reliance on storage and backup systems. Thus, reductions in PV cost alone may not significantly lower the overall NPC unless complemented by improvements in energy storage or system design that better address intermittency.

The sensitivity analyses in Fig. 10a and Fig. 10b show that the NPC varies inversely with the discount rate, with a ±6.47% change in NPC for a ±20% variation in discount rate for Zambian conditions and 6.72% for regional conditions respectively. While this trend aligns with general financial principles, that lower discount rates reduce investment costs, the magnitude of sensitivity observed here is relatively modest. This suggests that although favorable financing conditions can support renewable energy projects, other factors such as battery and PV costs (which exhibited greater sensitivity) may play a more dominant role in influencing the overall system economics.

Similar trends for variation in these parameters with NPC are found by Ramesh and Saini (2021) and Dhavala *et al.* (2021),

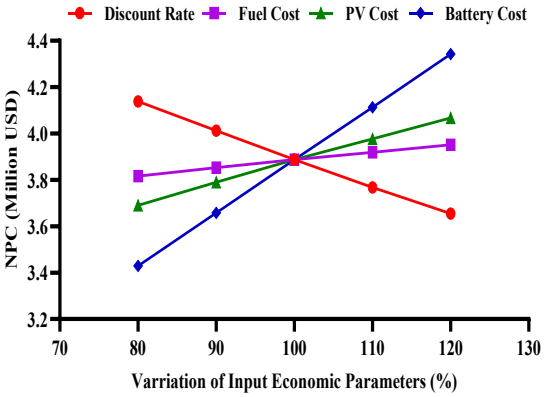

Fig. 10a NPC Variation with Input Parameters - Zambian Conditions

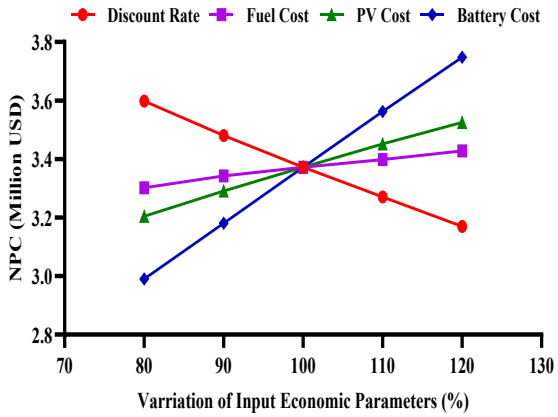

Fig. 10b: NPC Variation with Input Parameters - Regional Conditions

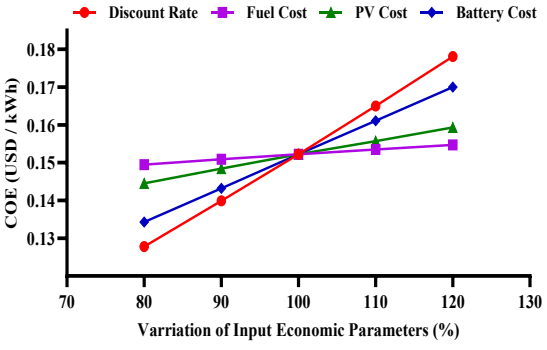

Fig. 10c: COE Variation with Input Parameters - Zambian Conditions

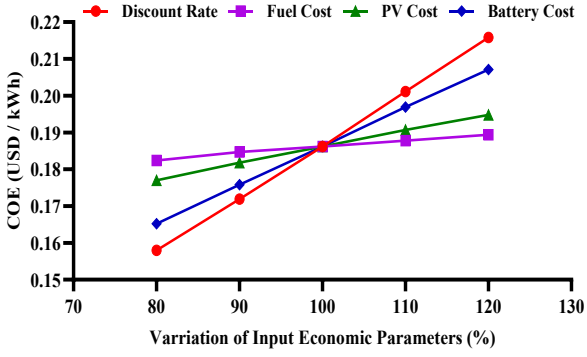

Fig 10d: COE Variation with Input Parameters - Regional Conditions

Fig. 10 Effect of change in input economic parameters on NPC and COE

although in varied magnitudes. These differences in magnitude highlight those specific parameters such as the efficiency and cost of the selected components (e.g., PV panels, batteries) and the site-specific resource availability (e.g., solar irradiance, wind speed), have a direct and substantial influence on the economic outcomes. For example, a location with higher solar isolation can reduce the required PV array size, thereby lowering capital costs, while the selection of more efficient but costlier batteries can shift the NPC depending on local energy storage needs and dispatch strategies.

4.6.2. Effect of Change in Input Economic Parameters on COE

Figs. 10c and 10d show the variation of PV cost, battery cost, fuel cost, and discount rate with the Cost of Energy (COE). It is seen that the COE varies in direct proportion to the changes in all these parameters. Among these parameters, the discount rate exhibits the most significant influence on COE of between ±8.08% and 16.03% for Zambian conditions and ±7.68 and 15.15% for regional conditions, as evidenced by its steeper slope. This highlights that financing-related variables, particularly the discount rate, can strongly impact on the affordability of energy in off-grid systems.

The pronounced sensitivity of COE to battery cost and discount rate, in both cases, emphasizes the importance of adopting cost-effective energy storage solutions and favorable financing mechanisms. These factors play a vital role in reducing the levelized cost of electricity for rural users and making hybrid renewable energy systems more viable, especially in underserved regions.

4.6.3. Effect of Change in Load Demand

To assess the impact of variations in load demand on NPC and RF, the load demand is varied by ±20 %. The proposed HRES is designed to efficiently manage these fluctuations while ensuring a reliable power supply. Fig. 11 illustrates how NPC and RF respond to changes in load demand under Zambian and regional conditions, respectively. As observed in Fig. 11a and Fig. 11b, for both cases, when the load is decreased by 10 % and 20 %, the NPC decreases almost proportionately. This is because a lower load demand reduces the energy required from the system, leading to lower operational costs and reduced reliance on backup sources, including the DG and batteries. However, when the load is increased by 10 % and 20 %, the NPC increases at a faster rate, approximately one and a half times the rate as indicated by the steeper slope. This disproportionate rise in cost is due to the HRES's reliance on batteries and the DG to meet the higher load demand under the Load Following (LF) strategy. The variation in NPC ranges from ±9.55 to 28.44% relative to the reference value for Zambian conditions and ±9.57% to 25.32% for regional conditions, highlighting the sensitivity of system costs to load fluctuations.

On the other hand, the RF, which represents the proportion of energy supplied by renewable sources, remains relatively stable when the load is reduced by 10 % and 20 %. This is because the HRES can meet the lower demand primarily using renewable energy sources (PV and wind) without significantly increasing the use of non-renewable backup systems. However, when the load is increased by 10 % and 20 %, the RF decreases. This decline occurs because the intermittent nature of solar PV power limits its ability to meet the higher demand. As a result, the additional load is primarily met by DG and batteries, which are non-renewable or storage-based sources. This shift reduces the overall renewable fraction of the system.

5. Conclusions

This study examined the techno-economic and environmental performance of multiple hybrid renewable energy system (HRES) configurations by varying PV panel capacities, battery technologies, and dispatch strategies. The findings demonstrate that replacing a diesel-only (DG) system with photovoltaic (PV)/wind-turbine (WT)/diesel-generator (DG)/biogas-generator (BG)/battery (BT), PV/DG/BT, PV/BG/BT and PV/BT as hybrid options can significantly contribute towards reducing both energy costs and pollutant emissions while considering appropriate technologies and ratings of the componentsts used, reinforcing the value of renewables for rural electrification.

Among the different configurations analyzed, the PV/DG/BT system consistently emerged as the most cost-effective solution, striking a practical balance between reliability and affordability. When broader economic and environmental considerations were integrated, the PV/WT/DG/BG/BT system offered a more balanced option, while systems with biomass integration proved particularly beneficial in reducing emissions. Larger-capacity PV modules (445 W) and advanced Li-ion batteries were found to deliver superior performance across all configurations, highlighting the importance of component selection in optimizing both cost and efficiency.

The sensitivity analysis further revealed that while all parameters influence system performance, battery cost and discount rate have the most significant impact on the overall economics of hybrid systems. This underlines the need for region-specific cost data and financing strategies to ensure realistic planning and deployment. Overall, the study confirms

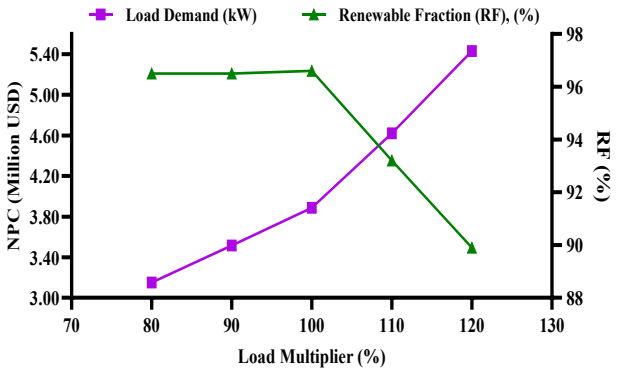

Fig 11a: NPC & RF Variation with Load Demand - Zambian Conditions

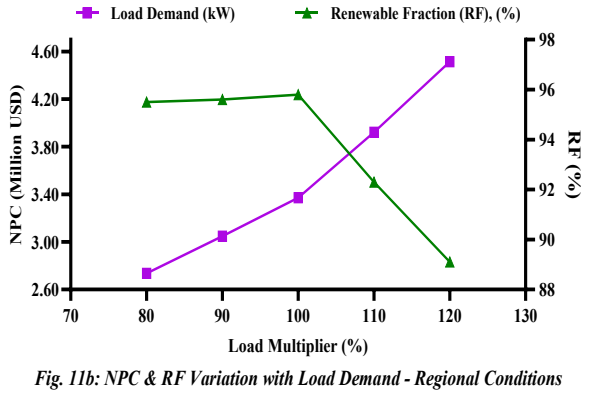

Fig. 11b: NPC & RF Variation with Load Demand - Regional Conditions

Fig. 11 Effect of change in load demand on NPC and RF

that carefully designed hybrid systems, supported by appropriate component choices and dispatch strategies, can provide reliable, affordable, and sustainable electricity for rural communities.

Acknowledgements

The Authors would like to acknowledge the University of Zambia (UNZA) for contributing its facilities towards this research work.

Author Contributions: A.A. Mr. Satnam S. Virdy, Prof. Francis D. Yamba, and Ramesh Mala: Conceptualization, methodology, formal analysis, writing—original draft, B.B. Prof. Francis D. Yamba, Dr. Isaac N. Simate; Prof. Manish Mishra; supervision, resources, project administration, C.C. Mr. Satnam S. Virdy, Prof. Yamba, Dr. Edwin Luwaya, and Dr. Simon Tembo; writing—review and editing, project administration, validation, DD. Prof. Shabbir Gheewala, Prof. Ramesh Mala and Dr. Mwansa Kaoma; writing—review and editing, project administration, validation. All authors have read and agreed to the published version of the manuscript.

Funding: The authors received no financial support for the research, authorship, and/or publication of this article.

Conflicts of Interest: The authors declare no conflict of interest

References

Abdulkarim A., Abdelkader S.M., Morrow D.J., Amuda S.A.Y., Madugu I.S., Falade A.J., Saminu S., Adediran Y.A. (2018) Effects of PV and Battery Storage Technologies on the Optimal Sizing of Renewable Energy Microgrid. *ELECTRIKA Journal of Electrical Engineering*, 17(1). Retrieved from www.electrika.utm.my.

Akhtari M.R. and Baneshi M. (2019) Techno-economic assessment and optimization of a hybrid renewable co-supply of electricity, heat and hydrogen system to enhance performance by recovering excess electricity for a large energy consumer. *Energy Conversions.* 188, 131-141.https://doi.org/10.1016/j.enconman.2019.03.067.

Babatunde O.M., Munda J.L. and Haman Y. (2020) A Comprehensive State of the Art Survey on Hybrid Renewable Energy System Operations and Planning. *IEEE Access,* 8, 75313-75346, https://doi.org/10.1109/ACCESS.2020.2998180.

Bahramara S., Moghaddam M. P. and Haghifam M. (2016) Optimal planning of Hybrid Renewable Energy Systems using HOMER: A Review. *Renewable and Sustainable Energy Reviews*, 62, 609-620. https://doi.org/10.1016/j.rser.2016.05.003.

Baneshi M., Hadianfard F. (2016) Techno-economic feasibility study of hybrid diesel/PV/ wind/battery electricity generation systems for non-residential large electricity consumers under southern Iran climate conditions. *Energy Conversions Management.* 127, 233-244. https://doi.org/10.1016/j.enconman.2016.09.008.

Bansal A.K. (2022) Sizing and forecasting techniques in photovoltaic-wind based hybrid renewable energy system: A review. *Journal of Cleaner Production*, 369, 133376. https://doi.org/10.1016/j.jclepro.2022.133376.

Bhatt A., Ongsakul W., and Madhu N.M. (2022) Optimal techno-economic feasibility study of net-zero carbon emission microgrid integrating second-life battery energy storage system. *Energy Conversion and Management,* 266, 115825. https://doi.org/10.1016/j.enconman.2022.115825.

Biramo I. (2020) Energy-Water-Agriculture Nexus Mini Grids to Power Rural Productive Hubs in Sub-Saharan Africa – A Case study of Walta Jalala Village in Bedeno Woreda of Ethiopia. *Master Thesis. European Solar Engineering School, Dalarna University*.

Bishoge O.K., Zhang L. and Mushi W.G. (2019) The Potential Renewable Energy for Sustainable Development in Tanzania: A Review. *Clean Technologies,* 1(1), 70-88. https://doi.org/10.3390/cleantechnologies1010006.

Bukar AI., Tan C.W., Lau K.Y. (2019) Optimal sizing of an autonomous photovoltaic/wind/battery/diesel generator microgrid using grasshopper optimization algorithm. *Solar Energy*, 188, 685-696. https://doi.org/10.1016/j.solener.2019.06.050.

Chauhan A., Saini R.P., (2016) Techno-economic feasibility study on Integrated Renewable Energy System for an isolated community of India. *Renewable and Sustainable Energy Reviews*, 59, 388–405. https://doi.org/10.1016/j.rser.2015.12.014.

Chaurasia R., Gairola S., Pal Y., (2022) Technical, economic, and environmental performance comparison analysis of a hybrid renewable energy system based on power dispatch strategies. *Sustainable Energy Technologies and Assessments*, 53, 102787. https://doi.org/10.1016/j.seta.2022.102787.

Das B.K., Hoque N., Mandal S., Pal T.K., Raihan M.A. (2017) A techno-economic feasibility of a stand-alone hybrid power generation for remote area application in Bangladesh. *Energy,* 134, 775-788. https://doi.org/10.1016/j.energy.2017.05.016.

Dhavala R.K., Suresh H.N. Rajanna S. and Ramesh M. (2021) Effects of different batteries and dispatch strategies on performance on standalone systems. *Energy Storage,* e306. https://doi.org/10.1002/est2.306 .

Dibaba H.D. (2019) Business model for micro grids in Sub-Saharan Africa Rural Areas: A case study in Revon C. Namibia. 2019. Master Thesis. https://lutpub.lut.fi/handle/10024/160125

Fofang T.F. and Tanyi E. (2020) Design and simulation of off grid solar/mini hydro renewable energy system using Homer Pro software: Case for Muyuka Rural Community, *IJERT*, 9(9), https://doi.org/10.17577/IJERTV9IS090294

Gabisa, E. and Gheewala, S. (2018) Potential of bio-energy production in Ethiopia based on available biomass residues. *Biomass and Bioenergy,* 111, 77–87. https://doi.org/10.1016/j.biombioe.2018.02.009.

Ganjei N., Zishan F., Alayi R., Somai H., Jahangiri M., Kumar R., Mohammadian A. (2022) Designing and Sesitivity Analysisof an Off-Grid Hybrid Wind Solar Power Plant with Diesel Generator and Battery Backup for the Rural Area in Iran. *Journal of Engineering*. https://doi.org/10.1155/2022/4966761 .

Hassan R., Das B.K. and Hasan M. (2022) Integrated off-grid hybrid renewable energy system optimization based on economic, environmental, and social indicators for sustainable development. *Energy*, 250, 123823. https://doi.org/10.1016/j.energy.2022.123823.

Heyine M.S., Yahya A.M., Daher D.H., Gaillard I., Menezo C., and Mahmoud A.K. (2022) Performance Evaluation of 50MWp Solar Plant under different Climate Conditions. *Int. J. Power Electron Drive Syst.,* 13(1), 561-575, https://doi.org/10.11591/ijpeds.v13.i1.pp561-575 .

HOMER Pro 3.14 (2020) User Manual Available from: https://support.ul-renewables.com/homer-manuals-pro/index.html [Accessed: 30th March 2024].

Iqbal M., Azam M., Naeem M., Khwaja A.S. and Anpalagan A. (2014) Optimisation, Classification, Algorithms and Tools for Renewable energy. A Review. *Renewable and Sustainable Energy Reviews*, 39, 640 – 654. https://doi.org/10.1016/j.rser.2014.07.120 .

IRENA Electrification Platform (IEP). (2024). https://accessplanning.irena.org/about .

IRENA (2025), Renewable Power Generation Costs (RPGC) in 2024, International Renewable Energy Agency, Abu Dhabi.

Kaoma M. and Gheewala S.H. (2021)a. Sustainability performance of lignocellulosic biomass-to bioenergy supply chains for Rural Growth Centers in Zambia. *Sustainable Production and Consumption,* 28, 1343 - 1365. https://doi.org/10.1016/j.spc.2021.08.007 .

Kaoma, M., Gheewala, S.H., (2021)b. Evaluation of the enabling environment for the sustainable development of rural-based bioenergy systems in Zambia. *Energy Policy*. 154, 112337. https://doi.org/10.1016/j.enpol.2021.112337 .

Kaoma, M. and Gheewala, S.H. (2020) Assessment of the bioenergy policy for the sustainable development of rural-based bioenergy systems in Zambia, *IOP Conference Series: Earth and Environmental Science,* 463(1). https://doi.org/10.1088/1755-1315/463/1/012012 .

Khan F.A., Pal N. Saeed S.H. and Yadav A. (2022) Modelling and techno-economic analysis of standalone SPV/Wind hybrid renewable energy system with lead-acid battery technology for rural applications. *Journal of Energy Storage* 55, 105742. https://doi.org/10.1016/j.est.2022.105742.

Khan F.A., Pal N., Saeed S.H. and Yadav A. (2022) Techno-economic and feasibility assessment of standalone solar Photovoltaic/Wind

hybrid energy system for various storage techniques and different rural locations in India. *Energy Conversion and Management*, 270, 116217. https://doi.org/10.1016/j.enconman.2022.116217.

Kumar P., Pal N. and Sharma H. (2022) Optimization and techno-economic analysis of a solar photo-voltaic/biomass/diesel/battery hybrid off-grid power generation system for rural remote electrification in eastern India. *Energy*, 247, 123560. https://doi.org/10.1016/j.energy.2022.123560.

Kumar P.P. Saini R.P. (2020) Optimization of an off-grid integrated hybrid renewable energy system with different battery technologies for rural electrification in India. *J Energy Storage*,3 2,101912. https://doi.org/10.1016/j.est.2020.101912.

Kumar S. and Rao S.K. (2022) Optimum capacity of hybrid renewable energy system suitable for fulfilling yearly load demand for a community building located at Vaddeswaram, Andhra Pradesh. *Energy & Buildings*, 277, 112570. https://doi.org/10.1016/j.enbuild.2022.112570.

Kushwaha P.K. and Bhattacharjee C. (2022) Integrated techno-economic-enviro-socio design of the hybrid renewable energy system with suitable dispatch strategy for domestic and telecommunication load across India. *Journal of Energy Storage* 55, 105340. https://doi.org/10.1016/j.est.2022.105340.

Li J., Liu P., Li Z. (2022) Optimal design and techno economic analysis of a hybrid renewable energy system for off-grid power supply and hydrogen production: A case study of West China. *Chemical Engineering Research and Design* 177, 604-614. https://doi.org/10.1016/j.cherd.2021.11.014 .

Mala R. and Saini R.P. (2020) Dispatch strategies-based performance analysis of a hybrid renewable energy system for a remote area in India. *Journal of Cleaner Production*. 259, 120697. https://doi.org/10.1016/j.jclepro.2020.120697 .

Mala R. and Saini R.P. (2020) Effect of different batteries and diesel generator on performance on a stand-alone hybrid renewable energy system. *Energy Sources, Part A: Recovery, Utilization and Environmental Effects*. (Online). https://doi.org/10.1080/15567036.2020.1763520 .

Micangeli A., Citto R., Kiva I.N., Santori S.G., Gambino V., and Kiplagot J. (2017) Energy production analysis and optimization of mini grid in remote areas: The case study of Habaswein, Kenya. *Energies,* 10, 1-23. https://doi.org/10.3390/en10122041.

Ministry of Energy. (2019) National Energy Policy. Lusaka. Ministry of Energy, Government Republic of Zambia.

Mwakitalima I.J., Rizwan M. and Kumar N. (2023) Integrating Solar Photovoltaic Power Source and Biogas Energy Based System for Increasing Access to Electricity in Rural Areas of Tanzania. *International Journal of Photoenergy*, ArticleID:7950699, http://doi.org/10.1155/2023/7950699 .

National Renewable Energy Laboratory (NREL). (2019). The Hybrid Optimisation Model for electric Renewables (HOMER). Available: www.homerenergy.com [Accessed: 6th March 2024).

Patel A.M. and Singal S.K. (2019) Optimal component selection of integrated renewable energy system for power generation in stand-alone applications. Energy. 175, pp 481-504. https://doi.org/10.1016/j.energy.2019.03.055.

Rai A., Shrivastava A., Jana K.C., Jayalakshmi N.S. (2021) Techno-economic environmental and sociological study of a microgrid for the electrification of difficult un-electrified isolated villages. *Sustainable Energy, Grids and Networks,* 28, 100548. https://doi.org/10.1016/j.segan.2021.100548.

Razmjoo A., Sumper A., Davarpanah A. (2019) Energy sustainability analysis based on SDGs for developing countries. *Energy Sources, Part A: Recovery, Utilization and Environmental Effects*. 42, 1041-56. https://doi.org/10.1080/15567036.2019.1602215.

Saha P., Kar A., Behera R.R., Pandey A., Chandrasekhar P., Kumar A. (2022) Performance optimization of hybrid renewable energy system for small scale micro-grid. *Materials Today: Proceedings,* 63, 527–534. https://doi.org/10.1016/j.matpr.2022.01.124.

Shane, A. and Gheewala, S.H. (2017) Missed environmental benefits of biogas production in Zambia. *Journal of Cleaner Production*, 142, 1200–1209. https://doi.org/10.1016/j.jclepro.2016.07.060.

Shane, A., Gheewala, S.H. and Phiri, S. (2017) Rural domestic biogas supply model for Zambia. *Renewable and Sustainable Energy Reviews,* 78, 683–697. https://doi.org/10.1016/j.rser.2017.05.008.

Singh S., Singh M., and Kaushik S.C. (2016) Feasibility study of an islanded microgrid in rural area consisting of PV, wind, biomass and battery energy storage system. *Energy Conversion and Management*. https://doi.org/10.1016/j.enconman.2016.09.046 .

Sinha S. and Chandel S.S. (2015) Review of recent trends in optimization techniques for solar photovoltaic-wind-based hybrid energy systems. *Renewable and Sustainable Energy Reviews*, 50, 755 – 769. https://doi.org/10.1016/j.rser.2015.05.040 .

Sudarsan K. and Sreenivasan G. (2022) PV Solar Farm as Static Synchronous Compensator for Power Compensation for Power Compensation in Hybrid System using Harris Hawks Optimizer Technique. Int. J. Power Electron Drive Syst., Vol. 13, No 1, pp 554-560, 2022. https://doi.org/10.11591/ijpeds.v13.i1.pp554-560.

The Sustainable Development Goals (SDG) Report (2023) [Online] United Nations. Available from: https://unstats.un.org/sdgs/report/2023/The-Sustainable-Development-Goals-Report-2023.pdf (Accessed 8th September 2023).

Viyaj V.K. (2016) Biogas is a Fit Option for Rural Energy. IIT, Delhi. Retrieved from http://Web.iitd.ac.in.

Virdy S.S. and Yamba F.D. (2013) An investigation into barriers affecting the implementation of the clean development mechanism (CDM) in Zambian firms. The Zambian Engineer. ISSN 1608-6678 Vol. 46, No. 1.

Werner U., Stohr U. and Hees N. (1989) Biogas Plants in Animal Husbandry: A Practical Guide. Published by Freider. Vieweg& Sohn VerlagsgesellschaftmbH, Braunschweig, Germany. ISBN: 3-52802048-2.

World Bank Open Data. (2023) Tracking SDG 7: The Energy Progress Report – Access to Electricity (% Population – Zambia). World Bank, Washington DC, World Bank Open Data. Available from: https://data.worldbank.org/indicator/EG.ELC.ACCS.ZS?locations=ZM [Accessed 5th September 2023].

Zala J.N. and Jain P. (2017) Design and optimization of a biogas-solar-wind hybrid system for decentralized energy generation for rural India. *International Research Journal of Engineering and Technology (IRJET).* 4(9). https://doi.org/10.15680/IRJET.2017.0409112.

Katti P.K. and Khedkar M.K. (2007) Alternative energy facilities based on site matching and generation unit sizing for remote area power supply. *Renewable Energy* 32 (8), 1346-1362. https://doi.org/10.1016/j.renene.2006.06.001.

Supplementary data

Table A1
Hourly load demand for the summer season

	Domestic							Commercial										Agric.
Appliance No.	1	2	3	4	5	6	7	1	2	3	4	5	6	7	8	9	10	11
Appliance	Bulb	TV	Fan	Fridge	Mobile Phone	Radio	Laptop	Bulb	TV	Fan	Fridge	Mobile Phone	Radio	Music System	Laptop	Electric Stove	Milling Plant	Water Pump
Rating (kW)	0.009	0.080	0.035	0.090	0.010	0.015	0.080	0.009	0.080	0.035	0.150	0.010	0.015	0.360	0.080	2.200	12.50	0.750
Qty	1926	535	535	214	1498	535	214	65	2	49	7	90	45	2	2	2	1	24
0:00	32.10	-	40.13	25.68	-	-	-	-	-	-	1.40	-	-	-	-	-	-	-
1:00	32.10	-	40.13	25.68	-	-	-	-	-	-	1.40	-	-	-	-	-	-	-
2:00	32.10	-	40.13	25.68	-	-	-	-	-	-	1.40	-	-	-	-	-	-	-
3:00	32.10	-	40.13	25.68	-	-	-	-	-	-	1.40	-	-	-	-	-	-	-
4:00	32.10	-	40.13	25.68	-	-	-	-	-	-	1.40	-	-	-	-	-	-	-
5:00	32.10	-	40.13	25.68	-	-	-	-	-	-	1.40	-	-	-	-	-	-	-
6:00	-	-	36.11	25.68	-	-	-	-	-	-	1.40	-	-	-	-	-	-	-
7:00	-	-	-	25.68	-	-	-	-	-	-	1.40	-	-	-	-	-	-	-
8:00	-	-	-	25.68	-	8.03	-	-	-	-	1.40	-	-	-	-	-	-	-
9:00	-	-	-	25.68	-	8.03	-	-	-	-	1.40	-	-	-	-	-	-	-
10:00	-	-	-	25.68	-	8.03	-	-	-	-	1.40	-	0.68	-	0.16	-	-	-
11:00	-	-	-	25.68	14.98	8.03	-	-	-	3.38	1.40	0.90	0.68	-	0.16	-	-	-
12:00	-	-	40.13	25.68	14.98	8.03	-	-	-	3.38	1.40	0.90	0.68	-	-	-	-	-
13:00	-	-	40.13	25.68	14.98	8.03	-	-	-	3.38	1.40	0.90	0.68	-	-	-	-	-
14:00	-	-	40.13	25.68	-	8.03	-	-	-	3.38	1.40	-	0.68	-	-	-	12.50	-
15:00	-	-	40.13	25.68	-	8.03	-	-	-	3.38	1.40	-	0.68	-	-	-	12.50	18.00
16:00	-	-	40.13	25.68	-	8.03	-	-	-	3.38	1.40	-	0.68	-	-	-	-	-
17:00	-	-	40.13	25.68	-	8.03	-	-	-	-	1.40	-	0.68	-	-	-	-	-
18:00	-	-	40.13	25.68	-	8.03	17.12	-	-	-	1.40	-	0.68	-	-	-	-	-
19:00	115.56	-	40.13	25.68	-	8.03	17.12	3.90	0.30	3.00	1.40	-	0.68	0.68	-	-	-	-
20:00	115.56	80.25	40.13	25.68	-	-	-	1.20	0.30	3.00	1.40	-	-	0.68	-	4.40	-	-
21:00	32.10	80.25	40.13	25.68	-	-	-	1.20	0.30	3.00	1.40	-	-	0.72	-	4.40	-	-
22:00	32.10	-	40.13	25.68	-	-	-	1.20	0.30	3.00	1.40	-	-	0.72	-	-	-	-
23:00	32.10	-	40.13	25.68	-	-	-	1.20	0.30	3.00	1.40	-	-	0.68	-	-	-	-

Table A1 Continued

	Community															
Appliance No.	1	2	1	4	5	6	7	8	9	10	11	12	13	14	15	
Appliance	60W Bulb	TV	Ceiling Fan	Large Fridge	Mobile Phone	Radio	HF Radio	Electric Stove	Office Equipment	Music Equipment	Medical Equipment	Dental Facility	Staff Houses	Water Pump	Street Light	Total Daily Hourly Load
Rating (kW)	0.009	0.080	0.750	0.150	0.010	0.015	0.800	2.200	0.000	0.000	0.000	1.200		0.750	0.030	
Qty	238	8	24	14	65	9	2	7	0	0	0	1	32	5	30	
0:00	1.84	-	0.96	2.80	-	0.05	-	-	-	-	0.60	-	-	-	9.00	114.55
1:00	1.84	-	0.96	2.80	-	0.05	-	-	-	-	0.60	-	-	-	9.00	114.55
2:00	1.84	-	0.96	2.80	-	0.05	-	-	-	-	0.60	-	-	-	9.00	114.55
3:00	1.84	-	0.96	2.80	-	0.05	-	-	-	-	0.60	-	-	-	9.00	114.55
4:00	1.84	-	0.96	2.80	-	0.05	-	-	-	-	0.60	-	-	-	9.00	114.55
5:00	0.48	-	0.96	2.80	-	0.05	-	-	-	-	0.60	-	-	-	9.00	113.19
6:00	-	-	0.96	2.80	-	0.05	-	4.40	2.00	-	-	-	-	-	-	73.39
7:00	-	-	0.96	2.80	-	0.05	-	6.60	2.04	-	-	-	-	-	-	39.52
8:00	-	-	0.96	2.80	-	0.11	1.60	4.40	6.00	-	2.00	-	-	-	-	52.97
9:00	-	-	0.96	2.80	-	0.08	-	-	6.32	-	0.25	-	-	-	-	45.51
10:00	-	-	1.56	2.80	-	0.14	-	-	7.32	1.58	0.87	1.20	-	2.25	-	53.65
11:00	-	-	1.56	2.80	0.65	0.08	-	-	9.72	1.58	0.87	1.20	-	-	-	73.65
12:00	-	0.75	1.56	2.80	0.65	0.08	-	15.40	6.52	-	-	-	-	-	-	122.91
13:00	-	0.75	1.56	2.80	0.65	0.08	-	-	2.04	-	-	-	-	-	-	103.03
14:00	-	-	1.56	2.80	-	0.08	-	4.40	11.20	-	0.25	-	-	-	-	112.06
15:00	-	-	1.56	2.80	-	0.08	-	-	13.04	-	0.25	-	-	2.25	-	129.75
16:00	-	-	1.56	2.80	-	0.08	1.60	-	8.32	-	0.25	-	-	0.75	-	94.63
17:00	-	-	1.56	2.80	-	0.08	-	-	2.00	-	-	-	-	-	-	82.34
18:00	2.70	-	3.96	2.80	-	0.05	-	-	-	-	-	-	-	-	-	102.53
19:00	20.46	0.60	3.96	2.80	-	0.05	-	11.00	1.00	1.82	-	-	-	-	9.00	267.15
20:00	20.46	0.60	3.96	2.80	-	0.05	-	-	1.00	1.58	0.60	-	-	-	9.00	312.64
21:00	17.76	0.30	3.96	2.80	-	0.05	-	-	-	-	0.60	-	-	-	9.00	223.64
22:00	17.76	0.30	0.96	2.80	-	0.05	-	-	-	-	0.60	-	-	-	9.00	135.99
23:00	3.34	-	0.96	2.80	-	0.05	-	-	-	-	0.60	-	-	-	9.00	121.23

**The shaded line represents the peak load hour for the summer season*